JOURNAL OF PETROLOGY | VOLUME 47 | NUMBER 1 | PAGES 191–230 | 2006 | doi:10.1093/petrology/egi072

Chemistry of the Shiant Isles Main Sill, NW Scotland, and Wider Implications for the Petrogenesis of Mafic Sills

F. G. F. GIBB[1]* AND C. M. B. HENDERSON[2]

[1]DEPARTMENT OF ENGINEERING MATERIALS, UNIVERSITY OF SHEFFIELD, SHEFFIELD S1 3JD, UK

[2]SCHOOL OF EARTH, ATMOSPHERIC AND ENVIRONMENTAL SCIENCES, THE UNIVERSITY OF MANCHESTER, MANCHESTER M13 9PL, UK

RECEIVED NOVEMBER 12, 2004; ACCEPTED JULY 11, 2005
ADVANCE ACCESS PUBLICATION AUGUST 31, 2005

Major and trace element data for the Tertiary, Shiant Isles Main Sill, NW Scotland, are used to discuss its complex internal differentiation. Vertical sections through the sill exhibit sharp breaks in chemistry that coincide with changes in texture, grain size and mineralogy. These breaks are paired, top and bottom, and correspond to the boundaries of intrusive units, confirming a four-phase multiple-intrusion model based on field relations, petrography, mineralogy and isotopes. Whole-rock chemistry is consistent with this model and necessitates only minor revisions to the intrusive and differentiation mechanisms previously proposed. The rocks contain strongly zoned minerals (e.g. olivine $Fo_{70–5}$, clinopyroxene Mg# = 75–5, plagioclase $An_{75–5}$) indicating almost perfect fractional crystallization, but whole-rock compositions do not show such extreme variations. Thus, while residual liquids became highly evolved in situ, *they mainly became trapped within the crystal network and did not undergo wholesale inward migration. Some inward (mainly upward) concentration of residual liquids did occur to form a 'sandwich horizon', but the more volatile-rich, late-stage liquids that did not crystallize* in situ *appear to have migrated to higher levels in the sill to form pegmatitic horizons. Parental liquid compositions are modelled for the intrusive units and it is concluded that the original parent magma formed by partial melting of upper mantle that was more depleted in LREE than the sources of most Scottish Tertiary basaltic rocks. Incompatible trace elements in the picrodolerite–crinanite intrusive unit support isotope evidence that its parent magma was contaminated by crustal material. Attempts to reconcile the chemical characteristics of the sill with a recently proposed petrogenetic model based on a single intrusion of magma differentiated by novel, but controversial, processes fail comprehensively. It is predicted that the complex petrogenetic history of the Shiant Isles sill is not unusual and could become the model for other large (>50 m thick) sills.*

KEY WORDS: *alkali basalt; differentiation; geochemistry; multiple intrusion; Shiant Isles; sill*

INTRODUCTION

Outcropping on the Shiant Isles, 24 km north of the Isle of Skye (Fig. 1), and intruded into Lower Jurassic sediments are some of the most northerly members of the Paleocene 'Little Minch Sill Complex' (Gibb & Gibson, 1989). It has long been recognized that the largest of these, termed the Shiant Isles Main Sill by Gibb & Henderson (1984), and hereafter referred to as the sill, is internally differentiated. It has often been cited as an example of the differentiation of mildly alkaline basaltic magma (e.g. Wager & Brown, 1967; Deer *et al.*, 1978; Gibson & Jones, 1991). Initially, the differentiation was attributed (Walker, 1930) to simple gravitative settling of olivine within a single intrusion of mafic magma. However, as new facts and evidence emerged over a series of papers, notably Drever (1953), Johnston (1953), Murray (1954*a*), Drever & Johnston (1959, 1965), Gibb (1973), Gibb & Henderson (1989, 1996), Foland *et al.* (2000) and Henderson *et al.* (2000), there has been an evolution in petrogenetic thinking and the sill is now regarded as a multiple intrusion. Ever more detailed models of emplacement and differentiation have arisen based on field, petrographic, mineralogical and isotopic data but, although all post-1980 models have been constrained by knowledge of the whole-rock chemistry, no comprehensive account of the internal chemistry of this classic sill has been published. [For an account of the natural and human history of the Shiant Isles, see Nicolson (2001).]

*Corresponding author. Telephone: ++(0)114 222 3630. Fax: ++(0)114 222 5943. E-mail: F.Gibb@shef.ac.uk

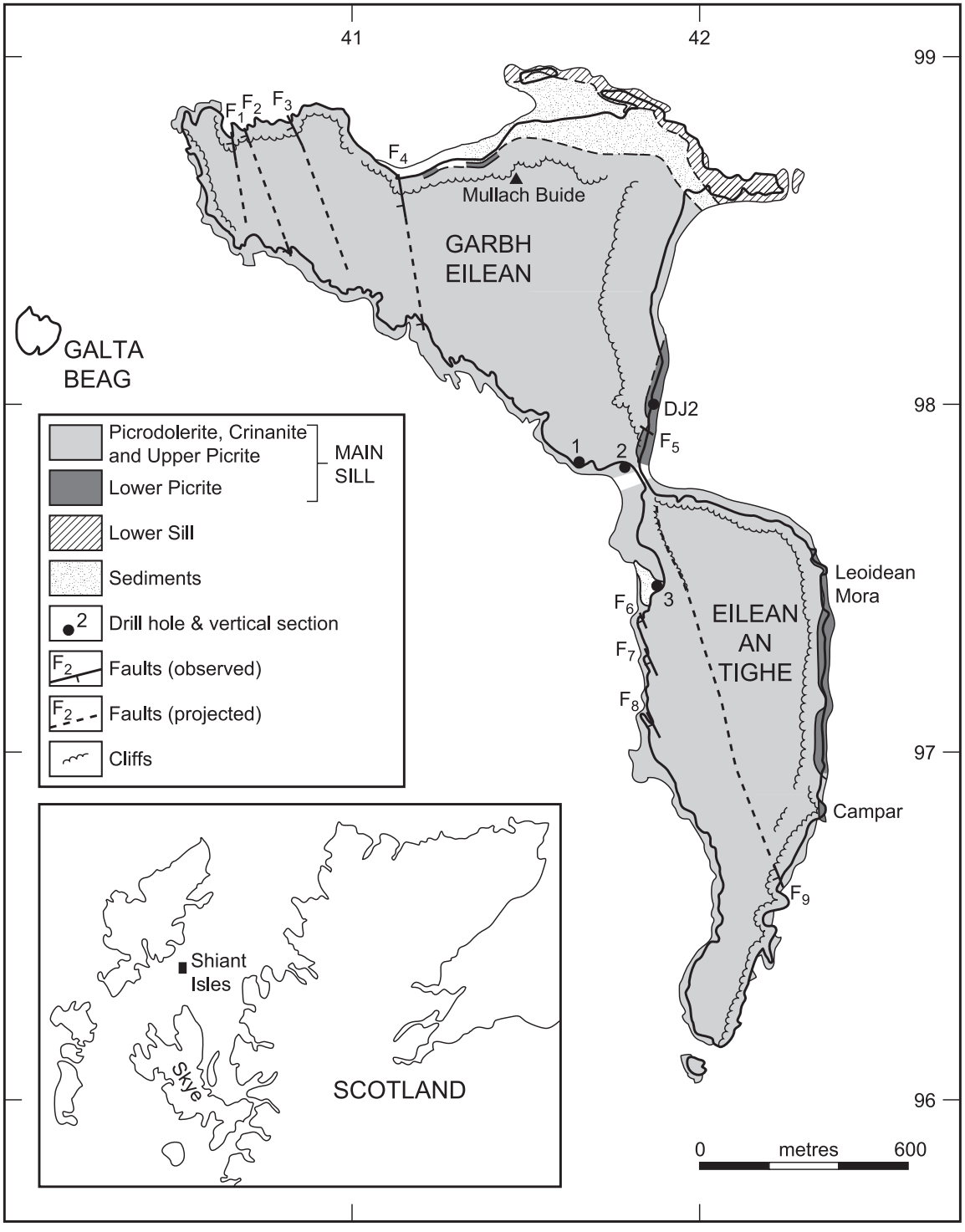

Fig. 1. Map of Garbh Eilean and Eilean an Tighe showing the outcrop of the Shiant Isles Main Sill and the locations of vertical sections and drill-holes (after Gibb & Henderson, 1996).

Here, we describe and discuss the major and trace element whole-rock chemistry of the sill and demonstrate how it controls and underpins our preferred genetic model of multiple intrusion, magma mixing, crustal contamination and post-intrusive processes (Foland *et al.*, 2000; Henderson *et al.*, 2000). We also provide a database of bulk-rock chemical analyses (Table 1) against which other petrogenetic processes and models for sills and

Table 1: Analyses of the Shiant Isles main sill

Specimen number:	oS82/69	S82/68	S82/67	S81/35	S81/34	S81/32	S81/31	S81/27	S81/24	S81/19
Section through sill:	2	2	2	2	2	2	2	2	2	2
Vertical height (m):	103·02	90·83	88·70	70·96	66·75	50·90	48·95	35·97	26·67	15·67
Composite section height (m):	132·92	120·73	118·60	100·86	96·65	80·80	78·85	65·87	56·57	45·57
Rock type:	Crin	Crin	Crin	Crin	Crin	Crin	Crin	P′dol	P′dol	P′dol
SiO_2 (wt %) by XRF or *ES*	47·48	47·85	47·32	46·81	47·02	48·09	47·52	46·04	46·32	46·32
TiO_2 (wt %) by XRF or *ES*	2·18	1·81	2·11	2·24	1·81	1·81	1·80	1·46	1·34	1·30
Al_2O_3 (wt %) by XRF or *ES*	15·31	16·84	16·75	15·58	16·97	16·45	15·98	15·96	16·56	17·72
$Fe_2O_3^T$ (wt %) by XRF or *ES*	14·14	11·85	13·42	14·74	12·73	12·25	11·80	13·83	12·75	11·42
Fe_2O_3 (wt %) by difference	4·14	3·49	3·51	5·23	4·52	2·98	3·58	3·06	2·75	2·58
FeO (wt %) by wet chemistry	9·00	7·52	8·92	8·56	7·39	8·34	7·40	9·69	9·00	7·95
MnO (wt %) by XRF or *ES*	0·20	0·17	0·20	0·22	0·19	0·19	0·18	0·20	0·18	0·16
MgO (wt %) by XRF or *ES*	4·96	4·74	4·27	4·39	5·27	5·13	5·79	8·23	9·17	8·32
CaO (wt %) by XRF or *ES*	11·51	12·63	11·66	10·82	11·64	12·47	12·54	10·74	10·72	11·24
Na_2O (wt %) by XRF or *ES*	3·12	2·95	3·14	3·43	2·93	2·95	2·83	2·71	2·52	2·48
K_2O (wt %) by XRF or *ES*	0·49	0·38	0·47	0·52	0·42	0·40	0·31	0·34	0·30	0·30
P_2O_5 (wt %) by XRF or *ES*	0·17	0·16	0·18	0·21	0·16	0·16	0·12	0·13	0·13	0·12
S (wt %) by XRF or *ES*	0·00	0·00	0·00	0·00	0·03	0·04	0·02	0·03	0·00	0·00
H_2O^+ (wt %) by wet chemistry	1·61	1·46	1·78	1·38	1·47	1·35	1·78	1·30	0·79	0·96
CO_2 (wt %) by wet chemistry	0·03	0·05	0·02	0·26	0·06	0·06	0·04	0·04	0·08	0·15
V (ppm) by XRF or *ICP-MS*	433	370	385	383	375	380	422	284	252	248
Cr (ppm) by XRF or *ICP-MS*	83	281	60	58	139	247	328	166	177	177
Co (ppm) by ICP-MS			51	60					74	
Ni (ppm) by XRF or *ICP-MS*	58	57	48	50	59	59	67	162	195	172
Cu (ppm) by XRF or *ICP-MS*	180	140	175	195	146	154	140	138	114	99
Zn (ppm) by XRF or *ICP-MS*	94	80	92	102	83	78	77	81	77	67
Ga (ppm) by ICP-MS			19·0	20·0					17·2	
Rb (ppm) by ID, *XRF* or (*ICP-MS*)	(*8·3*)	8·71	*13·0*	9·38	(*7·9*)	9·28	(*5·0*)	*6·0*	5·75	*7·0*
Sr (ppm) by ID, *XRF* or (*ICP-MS*)	*222*	242	(*242*)	240	*223*	224	*228*	*236*	232	*244*
Y (ppm) by XRF or *ICP-MS*	34	31	33	35	31	36	26	24	23	22
Zr (ppm) by XRF or *ICP-MS*	131	126	131	140	125	112	98	99	93	90
Nb (ppm) by XRF or *ICP-MS*	4·64	*4·0*	5·54	5·39	4·17	*5·0*	3·34	*4·0*	3·47	*4·0*
Ba (ppm) by XRF or *ICP-MS*	165	121	150	150	137	119	128	116	102	98
Hf (ppm) by ICP-MS	3·93		3·84	5·15	2·95		2·28		3·23	
Ta (ppm) by ICP-MS	0·41		0·27	0·77	0·35		0·22		0·26	
Pb (ppm) by ICP-MS			3·33	4·14					1·39	
Th (ppm) by ICP-MS	0·98		1·14	0·98	0·66		0·45		0·53	
U (ppm) by ICP-MS			0·18	0·22					0·15	
La (ppm) by ICP-MS	10·02		9·21	10·60	7·50		5·39		6·54	
Ce (ppm) by ICP-MS	24·15		23·88	28·40	18·11		13·17		17·24	
Pr (ppm) by ICP-MS	3·71		3·22	3·81	2·78		2·13		2·38	
Nd (ppm) by ICP-MS	18·55		16·68	20·10	14·14		11·01		12·52	
Sm (ppm) by ICP-MS	5·49		5·04	6·22	4·15		3·37		3·84	
Eu (ppm) by ICP-MS	1·92		1·91	2·28	1·57		1·37		1·51	
Gd (ppm) by ICP-MS	6·31		6·08	7·46	5·21		4·41		4·65	
Tb (ppm) by ICP-MS	1·08		1·06	1·31	0·95		0·77		0·82	
Dy (ppm) by ICP-MS	6·59		6·45	7·96	5·51		4·76		5·02	
Er (ppm) by ICP-MS	3·60		3·78	4·67	2·92		2·48		2·95	
Yb (ppm) by ICP-MS	3·42		3·17	3·83	2·69		2·27		2·43	
Lu (ppm) by ICP-MS	0·50		0·49	0·60	0·37		0·30		0·38	

Table 1: continued

Specimen:	S81/15	S81/14	S81/12	S81/11	SC486	SC492	SC518	SC533	SC534	SC543	SC560	SC574
Section:	2	2	2	2	2	2	2	2	2	2	2	2
Vertical ht.:	10·05	8·53	5·18	3·73	−2·98	−3·48	−6·27	−6·99	−7·09	−7·67	−8·74	−9·70
Composite ht.:	39·95	38·43	35·08	33·63	29·92	26·42	23·63	22·92	22·81	22·23	21·16	20·20
Rock type:	P′dol	P′dol	P′dol	P′dol	P′dol	P′dol	P′dol	P′dol	P′dol	LFP	LFP	LFP
SiO_2	45·49	45·39	44·86	45·05	42·26	41·72	41·99	41·12	39·25	40·49	42·15	40·86
TiO_2	1·08	1·12	0·95	0·94	0·76	0·66	0·78	0·65	0·79	1·32	1·12	1·03
Al_2O_3	16·68	15·89	14·59	14·65	9·75	9·62	9·05	8·41	7·46	9·34	8·14	8·30
$Fe_2O_3^T$	11·53	12·29	12·70	12·51	14·41	14·10	14·71	15·01	15·08	13·53	15·59	14·99
Fe_2O_3	2·04	1·93	1·64	2·25	2·32	3·03	2·75	2·96	3·74	3·44	3·28	3·08
FeO	8·54	9·32	9·95	9·23	10·88	9·96	10·76	10·84	10·20	9·08	11·08	10·72
MnO	0·16	0·18	0·17	0·17	0·19	0·18	0·19	0·19	0·20	0·17	0·20	0·19
MgO	11·12	11·65	14·72	14·62	24·06	24·81	24·79	25·55	27·15	23·82	23·62	26·19
CaO	10·44	10·42	9·45	9·65	6·52	6·09	6·38	6·33	5·25	6·27	6·70	5·16
Na_2O	2·31	2·06	1·83	1·91	1·38	1·35	1·25	1·15	1·05	1·69	1·39	1·26
K_2O	0·26	0·26	0·22	0·24	0·09	0·08	0·11	0·09	0·11	0·12	0·10	0·08
P_2O_5	0·09	0·11	0·08	0·05	0·05	0·07	0·05	0·05	0·09	0·15	0·07	0·07
S	0	0·01	0·08	0·05	0·04	0·02	0·00	0·03	0·02	0·02	0·03	0·10
H_2O^+	1·24	0·97	0·92	1·18	1·86	2·39	1·88	2·32	4·07	3·50	2·04	2·41
CO_2	0·26	0·11	0·05	0·06	0·09	0·16	0·21	0·18	0·21	0·18	0·11	0·18
V	226	230	203	203	168	152	186	167	167	192	248	182
Cr	210	243	354	412	1463	1607	1555	1558	1685	1190	1339	1593
Co	78			98	154		199		147	138		
Ni	289	312	480	468	907	978	1034	1085	1204	855	987	1249
Cu	71	89	212	127	102	95	85	250	146	138	84	424
Zn	69	75	76	74	85	79	91	86	89	80	100	86
Ga	16·3			14·5	11·3		11·4		13·0	16·1		
Rb	4·91	(*4·6*)	*4·0*	4·26	2·25	(*2·2*)	2·95	5·62	(*5·9*)	(*5·8*)	2·70	*1·0*
Sr	265	*229*	*217*	250	129	*118*	170	159	*113*	*136*	151	*126*
Y	20	19	17	16	11	11	12	10	13	24	15	13
Zr	82	76	67	61	49	53	58	48	73	102	66	67
Nb	3·10	2·31	*3·0*	1·86	1·15	1·02	1·55	1·04	2·01	2·84	1·81	*2·0*
Ba	76	88	77	68	50	39	51	45	41	45	43	40
Hf	2·96	1·69		1·95	0·82	1·22	1·76	1·41	1·41	1·90	2·04	
Ta	0·21	0·27		0·11		0·12	0·12	0·17			0·15	
Pb	1·82			1·23	1·42		0·96		1·71	1·47		
Th	0·44	0·36		0·43		0·22	0·39	0·31			0·26	
U	0·13			0·08			0·10					
La	5·54	4·46		4·16		2·18	3·09	2·04			3·31	
Ce	14·94	10·70		10·72		5·68	8·24	5·74			8·98	
Pr	2·10	1·71		1·54		0·98	1·18	0·93			1·59	
Nd	11·36	8·49		8·24		5·31	6·44	5·12			8·71	
Sm	3·57	2·46		2·63		1·63	2·12	1·73			2·97	
Eu	1·46	0·96		1·11		0·72	0·86	0·69			1·06	
Gd	4·29	3·02		3·19		1·99	2·65	2·12			3·62	
Tb	0·77	0·56		0·57		0·35	0·47	0·35			0·63	
Dy	4·71	3·30		3·42		2·14	2·91	2·42			4·08	
Er	2·79	1·78		2·01		1·17	1·73	1·34			2·29	
Yb	2·29	1·63		1·65		1·16	1·45	1·29			2·05	
Lu	0·35	0·24		0·26		0·18	0·23	0·19			0·29	

Specimen:	SC598	SC656	SC681	SC737	SC758	SC760	SC765L	SC770	SC988	SC1000	SC1019	SC1027
Section:	2	2	2	2	2	2	2	2	3	3	3	3
Vertical ht.:	−11·99	−17·63	−21·20	−26·78	−28·80	−28·93	−29·41	−29·77	−1·50	−1·85	−3·20	−3·71
Composite ht.:	17·91	12·27	8·70	3·12	1·10	0·97	0·49	0·13	165·40	165·05	163·70	163·19
Rock type:	LFP	LFP	MFP	MFP	SFP	SFP	OT	OT	OT	OT	SFP	SFP
SiO_2	40·15	40·83	40·30	42·20	41·65	41·61	42·70	43·50	43·03	43·01	42·58	43·40
TiO_2	0·84	0·74	0·83	1·03	1·19	1·23	1·41	1·63	1·67	1·48	1·34	1·18
Al_2O_3	7·65	8·24	8·95	11·23	11·94	11·95	14·61	14·75	15·13	16·18	11·90	11·79
$Fe_2O_3^T$	15·66	15·14	15·22	14·32	14·03	14·71	13·70	13·95	13·86	13·04	14·72	14·39
Fe_2O_3	3·44	3·32	3·88	4·14	5·85	6·31	7·83	8·08	3·28	3·04	2·41	1·63
FeO	11·00	10·64	10·20	9·16	7·36	7·56	5·28	5·28	9·52	9·00	11·08	11·48
MnO	0·20	0·20	0·20	0·19	0·20	0·19	0·19	0·18	0·18	0·19	0·19	0·20
MgO	27·34	26·16	24·44	19·08	17·30	16·43	10·92	9·24	8·72	9·37	16·92	18·13
CaO	5·59	6·11	6·39	7·67	7·72	7·74	9·83	10·20	10·06	9·87	7·90	7·66
Na_2O	0·87	0·93	1·02	1·81	1·50	1·69	1·46	1·75	2·10	2·38	1·96	2·12
K_2O	0·05	0·04	0·04	0·08	0·09	0·10	0·11	0·19	0·22	0·20	0·13	0·17
P_2O_5	0·07	0·04	0·06	0·07	0·08	0·08	0·08	0·12	0·14	0·12	0·12	0·13
S	0·01	0·00	0·00	0·06	0·02	0·02	0·06	0·02	1·55	0·54	0·42	0·61
H_2O^+	2·41	2·23	3·32	3·04	4·63	4·88	5·01	4·57	4·99	4·35	3·03	1·69
CO_2	0·04	0·12	0·19	0·12	0·14	0·18	0·06	0·12	0·63	0·49	0·30	0·33
V	179	169	179	209	230	242				305	257	217
Cr	1762	1674	1446	986	792	821			*429*	1674	792	869
Co		283		124		125	72		89	72		131
Ni	1233	1113	1000	797	618	646	*301*		*213*	246	615	681
Cu	124	80	94	201	102	139	*151*		*149*	152	130	121
Zn	90	89	90	85	84	88	*89*		*92*	87	93	94
Ga		16·5		12·5		14·1	16·8		25·4	19·3		16·5
Rb	1·69	1·47	(*1·3*)	2·42	*1·0*	2·53	2·12		(*7·8*)	4·11	3·61	4·01
Sr	117	133	*123*	137	*170*	250	206		(*327*)	329	214	194
Y	11	10	11	18	16	16	*16*		*22*	21	19	23
Zr	51	51	52	80	69	70	*66*		*89*	87	87	108
Nb	1·30	1·34	1·14	1·76	*3·0*	1·96	1·71		2·89	2·04	2·38	3·43
Ba	25	29	31	44	29	37	32		*53*	46	56	59
Hf	1·51	1·40	1·37	1·74		1·96	2·04		2·18	2·15	2·64	3·01
Ta	0·32	0·15	0·21	0·96		0·49	0·18			0·14	0·22	0·18
Pb		1·01		0·44		1·04	1·47		1·94	1·23		0·46
Th	0·25	0·21	0·20	0·29		0·23	0·16			0·22	0·31	0·41
U		0·05		0·05		0·06	0·06			0·07		0·09
La	2·00	1·79	1·50	2·70		2·48	2·73			3·22	4·06	4·60
Ce	5·46	4·95	4·97	7·06		7·36	6·82			9·36	11·24	13·09
Pr	1·02	0·90	0·91	1·15		1·19	1·11			1·53	1·97	2·03
Nd	5·84	4·94	4·93	6·27		6·85	6·42			8·76	10·89	11·03
Sm	2·03	1·67	1·83	2·05		2·36	2·29			3·02	3·53	3·53
Eu	0·74	0·67	0·63	0·77		0·92	0·97			1·22	1·34	1·20
Gd	2·33	2·32	2·10	2·49		2·89	2·77			3·66	4·27	4·30
Tb	0·47	0·40	0·35	0·43		0·51	0·50			0·64	0·76	0·74
Dy	2·68	2·44	2·27	2·64		3·10	3·16			4·12	4·45	4·59
Er	1·46	1·46	1·28	1·52		1·73	1·73			2·29	2·52	2·59
Yb	1·37	1·34	1·20	1·30		1·46	1·27			1·98	2·28	2·27
Lu	0·20	0·21	0·18	0·20		0·22	0·18			0·28	0·34	0·34

Table 1: continued

Specimen:	SC1032	SC1037P	SC1038	SC1039 U	SC1040	SC1041	SC1054	SC1060T	SC1066	SC1081
Section:	3	3	3	3	3	3	3	3	3	3
Vertical ht.:	−4·42	−4·74	−4·85	−5·31	−5·53	−5·58	−7·47	−8·50	−9·12	−10·74
Composite ht.:	162·48	162·16	162·05	161·59	161·38	161·32	159·43	158·40	157·58	158·16
Rock type:	MFP	MFP	GOPd	GOPd	GOPd	GOPd	GOPd	GOPd	Peg.	Crin
SiO_2	42·74	41·97	43·90	45·22	*47·12*		43·89	*49·45*	42·79	46·24
TiO_2	1·03	1·02	1·60	1·72	*1·20*	*1·18*	1·19	*1·23*	4·83	1·45
Al_2O_3	10·46	10·48	15·80	16·42	*12·08*	*10·38*	17·73	*16·21*	10·84	15·75
$Fe_2O_3^T$	14·95	15·53	13·75	12·69	*14·29*	*14·70*	12·19	*12·10*	22·43	12·80
Fe_2O_3	2·06	2·77	2·46	2·47			2·85		7·72	4·26
FeO	11·6	11·48	10·16	9·20			8·40		13·24	7·68
MnO	0·21	0·22	0·19	0·18	*0·19*	*0·20*	0·16	*0·17*	0·33	0·18
MgO	21·25	21·08	8·51	8·43	*13·52*	*11·75*	9·84	*8·22*	4·93	7·65
CaO	7·02	6·64	10·80	11·18	*9·76*	*8·19*	10·69	*10·66*	9·46	12·13
Na_2O	1·76	1·70	2·79	2·63	*1·72*	*1·82*	2·07	*2·29*	2·97	2·43
K_2O	0·13	0·12	0·22	0·18	*0·17*	*0·18*	0·18	*0·24*	0·36	0·20
P_2O_5	0·12	0·11	0·17	0·14	*0·15*	*0·16*	0·08	*0·13*	0·21	0·17
S	0·16	0·14	0·67	0·10			0·03		0·24	0·03
H_2O^+	1·85	2·31	2·19	1·70			1·90		3·13	1·65
CO_2	0·18	0·16	0·37	0·12			0·18		0·42	0·60
V	197	210	*319*	301	*173*		341		385	392
Cr	1084	1046	*1898*	228	*4683*	*6034*	5673	*3511*	6	260
Co	242	134	112		376	169	170	429	77	90
Ni	845	874	*299*	192	*863*	*781*	357	*509*	44	125
Cu	112	156	*251*	145	*554*	*326*	204	*655*	242	172
Zn	96	101	*82*	85	*94*	*119*	90	*162*	181	79
Ga	21·5	18·9	19·0		23·4	26·1	28·7	32·0	21·7	21·0
Rb	3·59	(*8·5*)	8·73	4·56	(*6·5*)	(*7·0*)	3·13	3·50	(*6·7*)	3·52
Sr	*127*	*122*	265	245	(*168*)	(*190*)	361	436	*148*	204
Y	22	21	*27*	24	*16*	*17*	18	*22*	42	18
Zr	98	87	*115*	104	*67*	*65*	78	*256*	160	70
Nb	2·80	2·15	3·21	2·94	1·80	1·64	3·05	0·39	6·03	2·34
Ba	55	38	*91*	67	*38*	*45*	55	*117*	123	103
Hf	2·75	1·75	*3·84*	2·40	1·84	1·69	2·63	12·27	3·99	2·85
Ta	0·42		*0·37*	0·28	0·65		0·71	1·58	0·37	0·62
Pb	0·95	1·21	*0·75*		2·56	1·34	1·00	4·30	1·74	1·58
Th	0·52		*0·40*	0·30	0·46		0·41	0·39	0·57	0·27
U	0·17		*0·12*		0·28		0·09	0·39	0·13	0·12
La	5·57		5·06	4·18	2·77		4·47	5·14	7·10	2·70
Ce	16·10		14·84	11·36	7·70		11·91	12·88	18·65	7·08
Pr	2·72		2·35	1·95			1·77	1·86	2·72	1·03
Nd	15·30		13·34	10·62	6·75		9·62	9·82	14·79	5·54
Sm	4·98		4·44	3·27	2·45		3·11	3·31	4·82	1·72
Eu	1·64		1·67	1·32	0·93		1·21	1·58	1·79	0·78
Gd	5·60		5·44	4·18	2·94		3·79	3·95	6·00	2·12
Tb	1·00		0·93	0·76	0·50		0·65	0·71	1·01	0·34
Dy	6·43		5·75	4·60	3·10		4·04	4·52	6·35	2·17
Er	3·58		3·17	2·48	1·86		2·24	2·56	3·48	1·12
Yb	3·37		2·73	2·19	1·41		1·94	2·21	3·01	0·96
Lu	0·48		0·41	0·30	0·17		0·29	0·31	0·46	0·14

Specimen:	SC1115	SC1131	SC1160	SC1191	SC1337	SC1397	SC1464	SC1489	BHVO-1		BHVO-Rec.	
Section:	3	3	3	3	3	3	3	3				
Vertical ht.:	−12·70	−14·27	−18·19	−20·70	−33·17	−37·54	−41·88	−44·86				
Composite ht.:	154·20	152·63	148·71	146·20	133·73	129·36	125·02	122·04				
Rock type:	Peg.	Crin	Crin	Crin	Crin	Crin	Crin	Crin				
SiO_2	47·42	47·15	48·22	46·67	47·70	46·63	46·96	47·69	*49·26*		49·94	(0·54)
TiO_2	3·15	1·35	1·51	1·90	2·08	2·10	2·12	1·81	*2·67*		2·71	(0·06)
Al_2O_3	12·49	16·26	16·89	15·91	16·23	16·75	16·78	16·25	*13·99*		13·80	(0·21)
$Fe_2O_3^T$	18·26	13·11	11·83	15·10	12·61	14·12	14·11	12·37	*12·52*		12·23	(0·20)
Fe_2O_3	8·70	2·93	2·89	3·23	3·99	3·76	3·71	3·39				
FeO	8·60	9·16	8·04	10·68	7·76	9·32	9·36	8·08				
MnO	0·27	0·19	0·18	0·23	0·18	0·21	0·21	0·19	*0·17*		0·17	(0·01)
MgO	2·66	7·34	5·84	5·84	4·49	4·10	3·91	4·98	*7·36*		7·23	(0·22)
CaO	8·89	11·53	12·25	10·85	12·15	10·39	10·86	12·21	*11·67*		11·4	(0·17)
Na_2O	3·95	2·53	2·90	2·82	2·95	3·40	3·25	2·90	*2·45*		2·26	(0·07)
K_2O	0·91	0·22	0·31	0·33	0·38	0·48	0·46	0·36	*0·56*		0·52	(0·04)
P_2O_5	0·95	0·08	0·11	0·14	0·17	0·21	0·21	0·17	*0·32*		0·27	(0·03)
S	0·12	0·02	0·02	0·04	0·06	0·06	0·04	0·06				
H_2O^+	1·85	1·19	1·22	1·36	1·50	2·24	1·74	1·77				
CO_2	0·09	0·07	0·05	0·09	0·10	0·12	0·14	0·09				
V	55	339	359	376	433	345	358	375	*345*	*(23)*	317	(12)
Cr	4	206	223	151	119	47	44	184	*306*	*(16)*	289	
Co	64		62				54		*50*	*(6)*	45	(2)
Ni	20	114	77	74	45	49	42	52	*122*	*(19)*	121	
Cu	201	125	127	171	176	179	187	152	*147*	*(25)*	136	
Zn	161	82	78	98	88	103	100	85	*101*	*(14)*	105	(5)
Ga	24·1		19·6				19·2		*25*	*(1)*	21	(2)
Rb	23·1	*(4·3)*	6·78	*(6·4)*	9·00	*10·0*	*(8·5)*	*(6·9)*	*11*	*(1)*	11	(2)
Sr	219	*233*	281	*270*	274	*290*	*296*	*305*	*397*	*(12)*	403	(25)
Y	92	17	24	27	33	34	35	31	*24*	*(1)*	28	(2)
Zr	318	73	97	112	129	140	145	118	*162*	*(6)*	179	(21)
Nb	10·85	2·00	2·59	6·99	4·24	*5·0*	4·41	5·13	*14*	*(3)*	19	
Ba	284	106	105	112	184	152	144	141	*142*	*(13)*	139	(14)
Hf	10·32	1·60	2·25	3·01	3·77		4·88	2·80	*4·3*	*(0·6)*	4·4	(0·2)
Ta	0·78	0·15	0·12	1·23	0·35		0·29	0·82	*2*	*(1)*	1·2	
Pb	4·36		0·67				2·07		*3·8*	*(1·5)*	2·6	(0·2)
Th	1·64	0·34	0·41	0·76	0·93		1·06	0·61	*1·26*	*(0·21)*	1·1	
U	0·45		0·08				0·27		*0·51*	*(0·14)*	1·75	
La	23·09	4·14	4·71	6·86	9·44		9·69	7·29	*14·7*	*(0·7)*	16	(1)
Ce	62·77	9·91	12·05	16·11	21·35		24·81	17·50	*39*	*(2)*	39	(4)
Pr	8·74	1·54	1·72	2·47	3·29		3·55	2·70	*5·0*	*(0·3)*	5·26	
Nd	47·19	8·35	9·10	13·01	16·58		18·66	13·80	*24*	*(1)*	25	(2)
Sm	14·02	2·64	2·83	3·87	4·84		5·72	4·04	*6·1*	*(0·4)*	6·2	(0·3)
Eu	3·92	1·31	1·13	1·51	1·81		2·05	1·57	*2·1*	*(0·2)*	2·06	(0·08)
Gd	17·00	3·20	3·47	4·80	5·92		7·03	5·21	*6·1*	*(0·4)*	6·4	
Tb	2·78	0·57	0·58	0·83	1·00		1·24	0·88	*0·95*	*(0·08)*	0·96	
Dy	17·22	3·28	3·45	5·01	5·87		7·48	5·32	*5·5*	*(0·5)*	5·2	(0·3)
Er	9·38	1·75	2·04	2·71	3·28		4·21	2·88	*2·7*	*(0·2)*	2·42	
Yb	7·93	1·62	1·76	2·54	3·14		3·65	2·68	*2·1*	*(0·2)*	2·02	
Lu	1·18	0·23	0·26	0·37	0·50		0·61	0·36	*0·30*	*(0·05)*	0·29	

Rock types: Crin, crinanite; GOPd, granular olivine picrodolerite; P'dol, picrodolerite; OT, olivine teschenite; LFP, large-feldspar picrite; MFP, medium-feldspar picrite; SFP, small-feldspar picrite; Peg., pegmatite. Analytical methods: ES, emission spectroscopy; ICP-MS, inductively coupled plasma mass spectrometry; ID, isotope dilution; XRF, X-ray fluorescence spectrometry. Alternative methods indicated by *italics* and parentheses. $Fe_2O_3^T$, total Fe as Fe_2O_3. BHVO-1, USGS standard rock (Govindaraju, 1989) used as an internal standard. In rightmost column, figures in parentheses are 1σ values for five analyses (see text). BHVO-Rec, recommended values for BHVO-2.

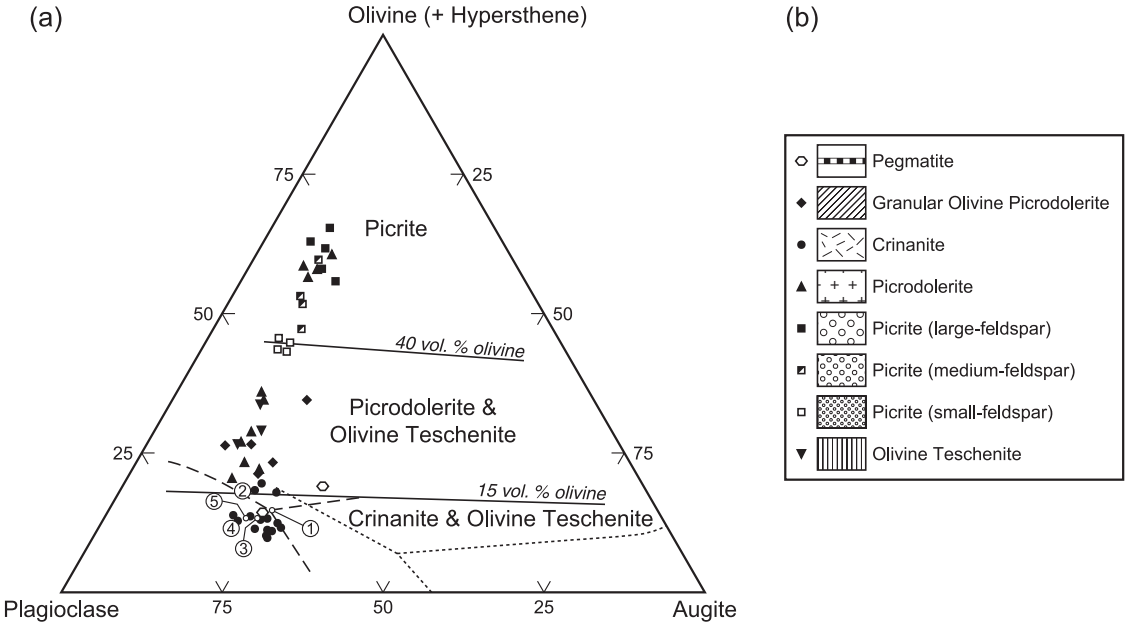

Fig. 2. (a) Relationships between the principal rock types in terms of olivine–plagioclase–augite (wt %). The petrographic divisions between picrite and picrodolerite and between picrodolerite and crinanite are at 40% and 15% modal olivine, respectively. Whole-rock analyses are plotted in terms of their CIPW norms (with hypersthene added to olivine). The dashed lines are the ternary cotectics determined for natural rocks at 5 kbar (Morse *et al.*, 2004) and the dotted lines are the cotectics for the pure end-member system Fo–Di–An at 1 atm (Osborn & Tait, 1952). Numbered circles are compositions of calculated parental liquids (see Table 2 and section on parental magmas) as follows: 1, PicrPL; 2, OTPL; 3, PdolPL1; 4, PdolPL2; 5, evolved crinanite. (b) Key to symbols and ornaments used for rock types throughout the paper.

other intrusions (e.g. Huppert & Sparks, 1980; Marsh, 1996; Latypov, 2003*b*) might be tested.

INTERNAL STRUCTURE

Rock names

The names crinanite, picrite, picrodolerite, teschenite and olivine teschenite have been used for the analcime-bearing mafic rocks of the Shiant Isles by all previous workers, albeit with some inconsistency. According to the IUGS classification (Le Maitre *et al.*, 1989), almost all the Shiant Isles rocks would be olivine gabbros, if regarded as plutonic, or picrites and picrite basalts, if volcanic. To avoid confusion, allow continuity and allow distinction between petrographic units we have elected to retain the original terms and define them as used in all our previous work on the sill (Gibb & Henderson 1984). This usage is summarized below and illustrated in terms of the three main mineral constituents in Fig. 2.

Teschenite = medium- to fine-grained rock consisting of plagioclase and clinopyroxene with minor analcime. Olivine teschenites can contain up to 20% olivine.

Crinanite = medium- to fine-grained rock consisting of olivine (<∼15%), plagioclase and clinopyroxene with minor analcime and with a distinctive ophitic or sub-ophitic olivine texture. This texture usually occurs in the sill at olivine contents below about 15% and its disappearance marks the transition from crinanite to picrodolerite.

Picrodolerite = medium- to fine-grained rock consisting of olivine (>∼15%), plagioclase and clinopyroxene with minor analcime.

Picrite = coarse- to fine-grained rock consisting of olivine (>40%), plagioclase and clinopyroxene, with or without minor analcime. Three petrographic variants have been identified in the Shiant Isles sill and distinguished as large-feldspar picrite, medium-feldspar picrite and small-feldspar picrite (Gibb & Henderson, 1989, fig. 5).

Within the petrographic units of the sill (below and Fig. 3), picrodolerites often grade into rocks that have slightly more than 40% olivine but are otherwise identical. Similarly, picrite units locally contain less than 40% olivine. To avoid overly rigid use of rock names, we introduced the convention of using single quotes to signify 'picrites' and 'picrodolerites' that have olivine contents lower and higher, respectively, than 40% (Gibb & Henderson, 1996).

Distribution

The thickness of the sill varies locally, with a maximum of ∼165 m. The main rock types are distributed as shown in the composite section (Fig. 3), which is based on sampled vertical sections through the sill, including cored

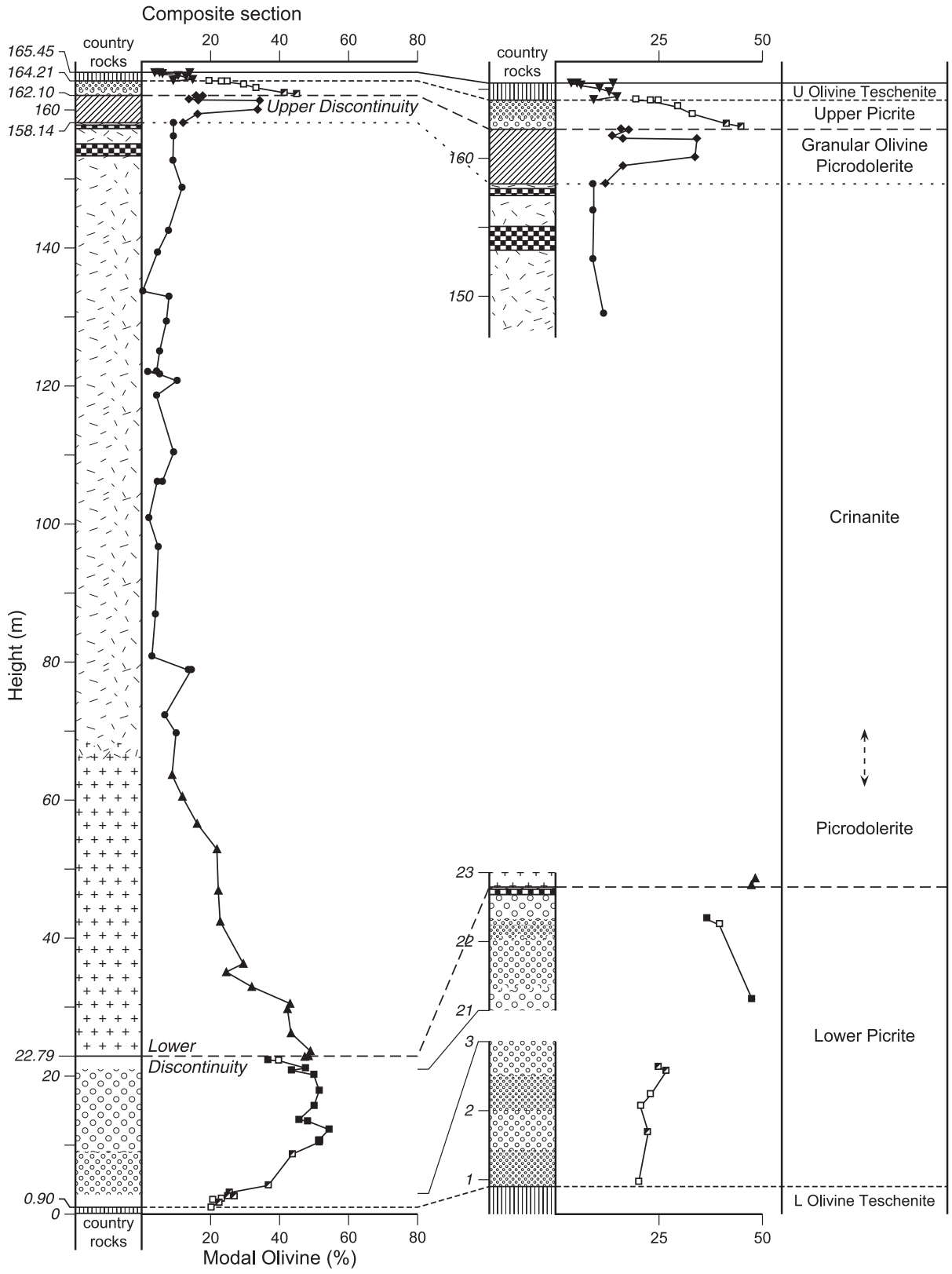

Fig. 3. Composite section through the sill showing the distribution of modal olivine, rock types and petrographic units. Ornaments and symbols as in Fig. 2b (after Gibb & Henderson, 1996; Henderson *et al.*, 2000).

drill-holes (Gibb & Henderson, 1996; Henderson *et al.*, 2000). The sill can be subdivided into a number of petrographic units, which are capitalized in the text and figures (e.g. Lower Picrite, Picrodolerite–crinanite) to distinguish them from rock types. These are shown in Fig. 3. The modal olivine profile is generally S-shaped (Gibb & Henderson, 1992) but with a second, upper maximum. It has been described by Latypov (2003*b*) as "double humped".

Emplacement

The field and petrographic relationships between the various internal subdivisions and their mineralogies led to the development of a four-phase multiple intrusion model (Gibb & Henderson, 1989, 1996; Foland *et al.*, 2000; Henderson *et al.*, 2000). This is summarized below and illustrated in Fig. 4.

(1) Emplacement into the sediments of magma that gave rise to the Upper and Lower Olivine Teschenites (Fig. 3). These have a combined thickness of just over 2 m, but the original intrusion was probably slightly thicker, its central part having been displaced by a subsequent intrusion (Fig. 4, Stage 2a). On emplacement, the marginal parts of the magma, which chilled against the sediments, contained ~14% of olivine phenocrysts. After emplacement, sinking of these phenocrysts occurred, especially from the upper parts of the unit, just below the chilled margin.

(2) Intrusion into (1), before it was completely solidified, of an olivine phenocryst-rich magma that subsequently formed the Upper and Lower Picrites with a total thickness around 24 m. During emplacement, there were substantial variations in the phenocryst content and minor variations in the composition of the suspending liquid. Both of these arose during tapping of the source magma chamber and uprise in the feeder conduit, and resulted in the internal differentiation of the Picrite unit. The Sr/Nd isotope ratios of the magmas that produced this unit and the Olivine Teschenite units (Stage 1) are indistinguishable, suggesting that both originated in the same deep magma chamber and probably gained access to the sill via the same feeder system.

(3) Intrusion of a substantial pulse of magma between the Lower Picrite and the Upper Picrite (Fig. 3) to form the 135 m thick Picrodolerite–crinanite unit. This gave rise to the Lower Discontinuity, which is a petrographic break visible in the drill-cores and conspicuous in the field (Gibb & Henderson, 1989, figs 3 and 4). A (presumed) similar upper contact (transient discontinuity; Fig. 4) between the new magma and overlying picrite has been obliterated by subsequent intrusion (Stage 4). At the time of emplacement, the adjacent picrite must have been a rigid crystal mush, cooler than the new magma to cause chilling, but still with sufficient interstitial liquid to allow extensive subsequent mixing across the Lower Discontinuity (Gibb & Henderson, 1996; Foland *et al.*, 2000). However, the Sr/Nd isotope ratios were initially homogeneous throughout the Picrodolerite–crinanite unit and distinct from those of the Olivine Teschenite and Picrite units, suggesting a separate (albeit probably related), more evolved source (Foland *et al.*, 2000). This, together with the absence of xenoliths of olivine teschenite or picrite in the unit, could be an indication that the magma accessed the sill via a separate feeder system. The magma contained phenocrysts of olivine (~10%) and calcic plagioclase (~1%) that settled out after emplacement to differentiate the unit into picrodolerite passing upwards into crinanite (Fig. 3).

(4) Finally, a fourth intrusion of magma ascended through the country rock along a separate feeder dyke, becoming contaminated by the sediments. As it passed through the upper parts of the sill, it picked up xenoliths of more and less solidified crinanite before spreading out laterally along the junction between the top of the Picrodolerite–crinanite and the Upper Picrite to form the 4 m thick Granular Olivine Picrodolerite (abbreviated as GOPd). This intrusion eroded away the pre-existing crinanite–picrite contact before chilling against both adjacent units. The upper surface of the GOPd chilled against completely crystallized picrite to form the Upper Discontinuity (Fig. 3) but the underlying crinanite was still sufficiently 'mushy' to allow post-intrusive mixing of the liquid phases of the two magmas across the interface (Foland *et al.*, 2000). As intrusion of the GOPd progressed, the feeder dyke widened, reducing the amount of sediment contamination and increasing the flow rate and olivine phenocryst content of the magma. The last two enabled the onset of flow differentiation in the feeder, with the result that the magma was emplaced into the sill with an olivine-rich central 'plug'. This unit, which appears to be exposed only at the NW corner of Eilean an Tighe (Fig. 1), may not persist laterally throughout the whole sill.

The emplacement of all four magma pulses must have occurred over a relatively short time span, as each intrusion was emplaced before its immediate predecessor had completely solidified. One result of this was that after the intrusion of the GOPd, the sill underwent much of its remaining cooling as a single thermal unit, as evidenced by the continuity of the massive columnar joints across unit boundaries. During the later stages of this cooling, hydrothermal alteration and Sr exchange with the enclosing sediments occurred, the evidence of which is most marked in the marginal parts of the sill. These effects are most noticeable in the alteration of the primary feldspathic minerals to analcime and zeolites, alteration of olivine to serpentine and the local precipitation of sulphide minerals (Gibb & Henderson, 1996).

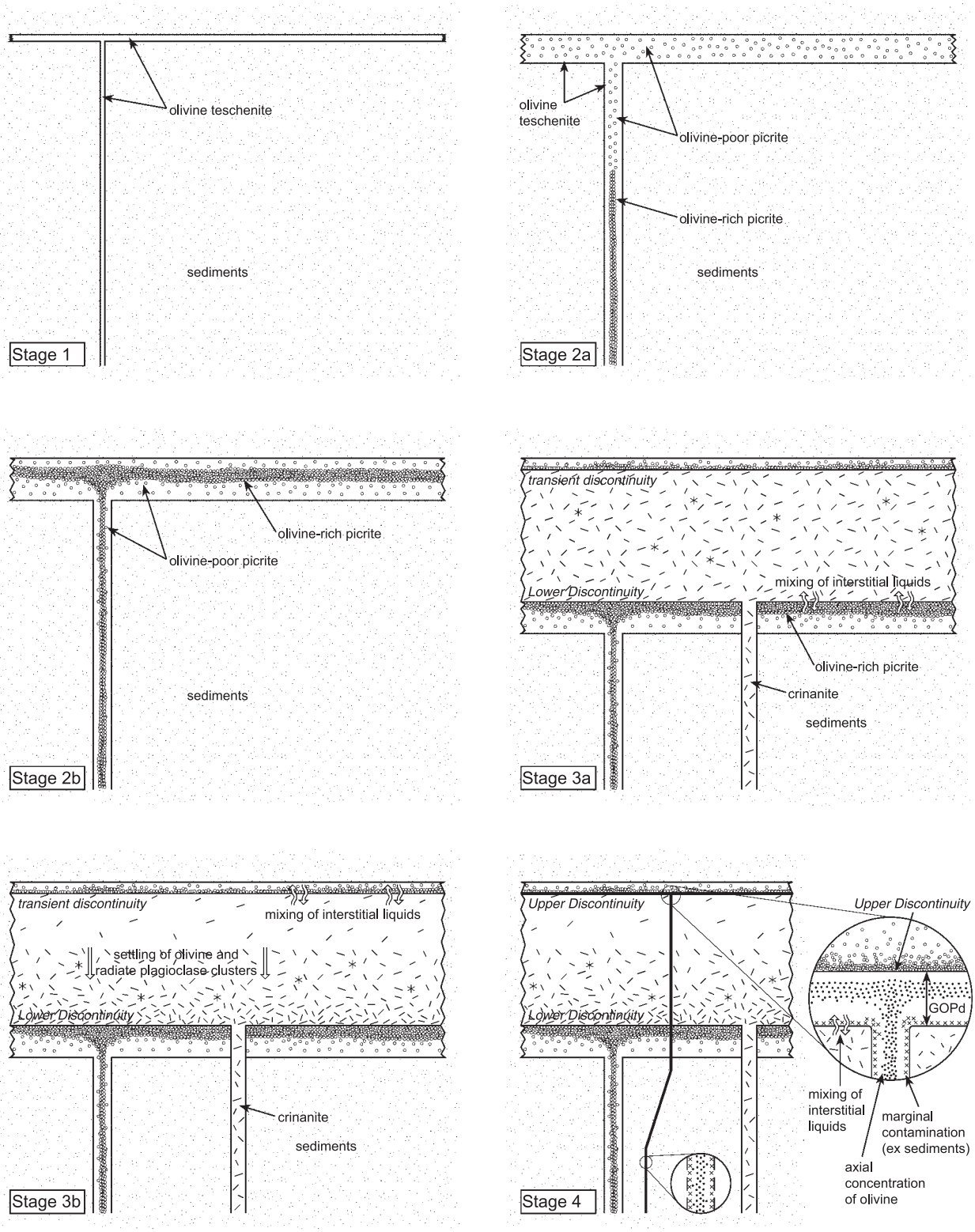

Fig. 4. Schematic illustration of the sequential emplacement of units into the sill (not to scale). Stage 1, Olivine Teschenites; Stage 2a, Picrites (early phase); Stage 2b, Picrites (later phase); Stage 3a, Picrodolerite–crinanite emplacement; Stage 3b, Picrodolerite–crinanite differentiation; Stage 4, Granular Olivine Picrodolerite.

Nd and Sr isotope data (Foland *et al.*, 2000) show that two distinct, albeit genetically related, magmas were involved in the formation of the sill. A more primitive, "picritic" magma, characterized by nine analysed picrites and olivine teschenites, has $^{143}Nd/^{144}Nd = 0{\cdot}51281$–$0{\cdot}51287$ ($2\sigma = 0{\cdot}00001$) and $^{87}Sr/^{86}Sr = 0{\cdot}7035$–$0{\cdot}7037$ ($2\sigma = 0{\cdot}0001$) and a more evolved "crinanitic" magma, characterized by 10 analysed picrodolerites and crinanites, has $^{143}Nd/^{144}Nd = 0{\cdot}51252$–$0{\cdot}51256$ ($2\sigma = 0{\cdot}00002$) and $^{87}Sr/^{86}Sr = 0{\cdot}7047$–$0{\cdot}7049$ ($2\sigma = 0{\cdot}0001$). The former was emplaced to form the Olivine Teschenite (Stage 1) and Picrite (Stage 2) units, while the latter gave rise to the Picrodolerite–crinanite (Stage 3). The emplacement of the GOPd (Stage 4) represented a return to the more primitive picritic magma, although with some contamination by the country rock and mixing with the crinanitic magma.

It has recently been suggested (Latypov, 2003*b*) that internally differentiated mafic–ultramafic sills with "double humped", S-shaped modal profiles like (and including) the Shiant Isles Main Sill are formed by intrusion of a single pulse of magma in which vigorous, wholesale internal turbulent convection becomes established. Notwithstanding the arguments against such convection occurring in sills (Marsh, 1989; Gibb & Henderson, 1992), Latypov proposed that it leads to very high-temperature gradients across liquid marginal boundary layers, enabling Soret diffusion to generate compositional variations that are the reverse of normal fractional crystallization. We shall show that the whole-rock chemistry, like the field and petrographic evidence, and the Sr–Nd isotope chemistry, is inconsistent with such an origin for the Shiant Isles sill.

ANALYTICAL METHODS

Sill rocks (151 samples) and their host sediments (four samples) were analysed for major elements and 31 trace elements (including REE), although not every sample was analysed for all elements. For 146 of the samples, major elements were determined at the University of Sheffield by X-ray fluorescence (XRF) analysis of lithium tetraborate fusion discs. Additionally, Fe^{2+} was determined by the ammonium metavanadate method of back-titrating excess metavanadate with standardized ferrous ammonium sulphate solution; CO_2 released by boiling concentrated phosphoric acid was adsorbed on 'Sofnolite' and weighed by difference and H_2O^+ released by heating was condensed and weighed. For eight samples, the major elements were determined by emission spectroscopy at the University of Manchester. For the majority of the samples, the trace elements V, Cr, Mn, Ni, Cu, Zn, Rb, Sr, Y, Zr, Nb and Ba were determined by XRF analysis of pressed powder pellets with 'SX' binder (van Zyl, 1982) at the University of Sheffield. For 50 samples, V, Cr, Co, Ni, Cu, Zn, Ga, Y, Zr, Nb, Ba, La, Ce, Pr, Nd, Sm, Eu, Gd, Tb, Dy, Er, Yb, Lu, Hf, Ta, Pb, Th, and U were determined by ICP-MS at the University of Manchester and for 32 samples, Rb, Sr, Nd and Sm were analysed by isotope dilution at Ohio State University, Columbus, USA. The ICP-MS analyses were carried out by a method based on that of Pearce *et al.* (1997) using a VG Elemental Plasmaquad 2 STE. Samples were digested in HF/HNO_3 in a C.E.M. MDS-2000 microwave system, transferred to PTFE basins, taken to dryness twice and finally taken up in 2% HNO_3. The ICP-MS data were normalized using the Sr value obtained by isotope dilution or XRF analysis.

Where the same trace elements were analysed by more than one of XRF, ICP-MS or isotope dilution, agreement for most elements is better than 10% (relative). The exceptions are some transition elements (mainly V, Cr and Ni) analysed by ICP-MS, which showed the effects of molecular interferences from Cl^- (from residual perchloric acid) or Ca-bearing complexes. For rocks with <5 ppm Rb and Nb, XRF data were unreliable. Consequently, we prefer XRF data for the transition elements, isotope dilution or ICP-MS data for Rb, and ICP-MS data for Nb.

The accuracy of the emission spectroscopy data for major elements and of the ICP-MS data for trace elements was assessed by analysing the USGS standard rock BHVO-1 with each batch of samples. The results for the standard are given in Table 1, together with the recommended values (Govindaraju, 1989) from which it can be seen that agreement is satisfactory except for our Ta values, which, consequently, have not been used.

Representative whole-rock analyses of the sill rocks are given in Table 1. Wherever we have values determined by more than one method, those for the preferred method are presented, as indicated in Table 1. Only REE values determined by ICP-MS have been used in the figures and for interpretations.

VERTICAL VARIATIONS IN WHOLE-ROCK CHEMISTRY

It has been known since the pioneering work of Walker (1930) that the sill is vertically differentiated. This is illustrated by the variations in major and trace element chemistry (Fig. 5) for the three vertical sections described by Gibb & Henderson (1996, figs 2 and 3). However, in subsequent discussions, we focus on vertical chemical variations in the context of the composite section constructed from these by Gibb & Henderson (1996) and Henderson *et al.* (2000) in order to provide an overall framework for petrogenetic discussion. By doing so, the important geochemical changes that occur inward from

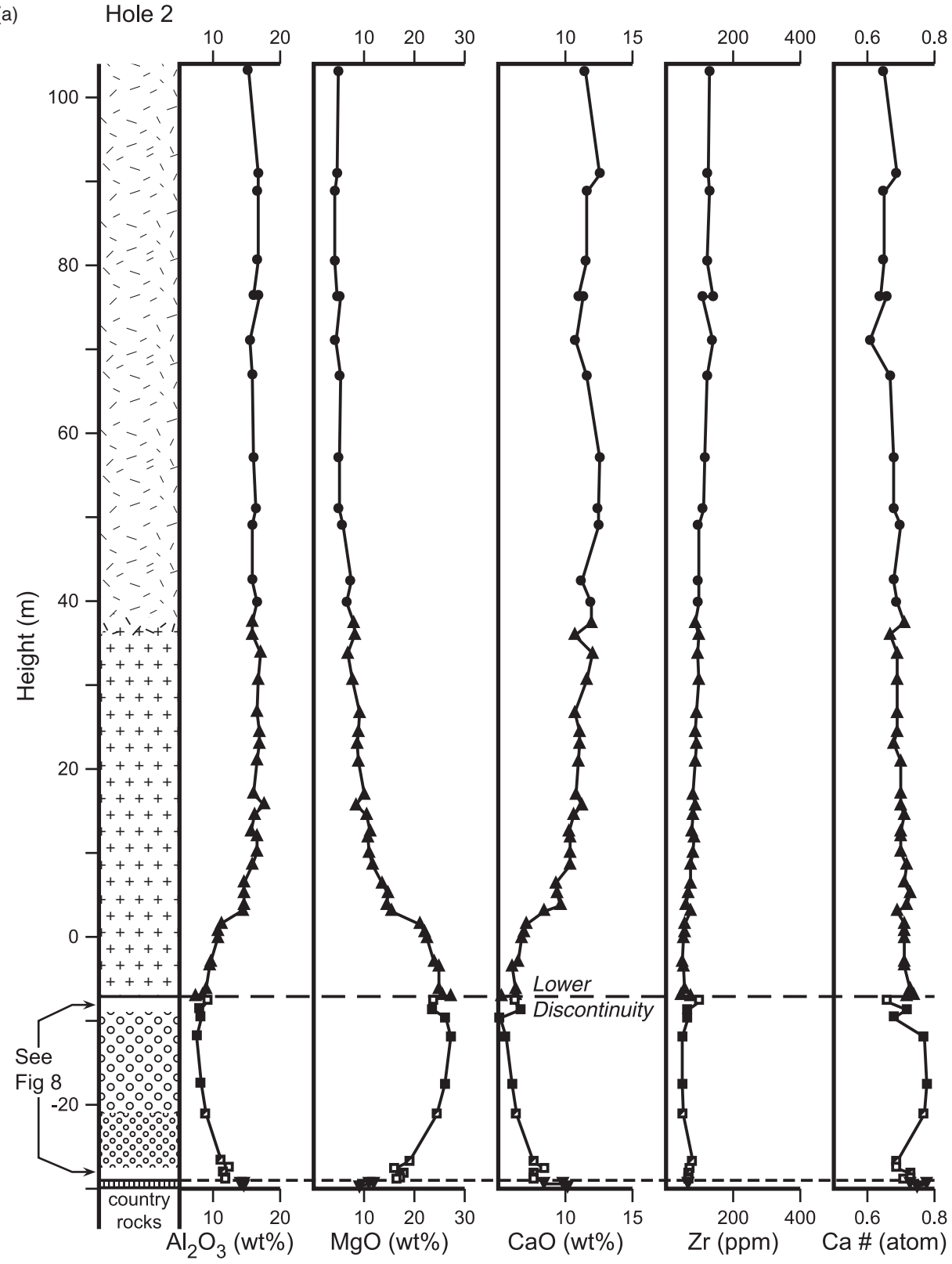

Fig. 5. Vertical variations in selected chemical parameters for (a) the Hole 2 section and (b) the Hole 1 and Hole 3 sections. Ca# = Ca/(Ca + Na + K) (atomic proportions). Symbols and ornaments as in Fig. 2b.

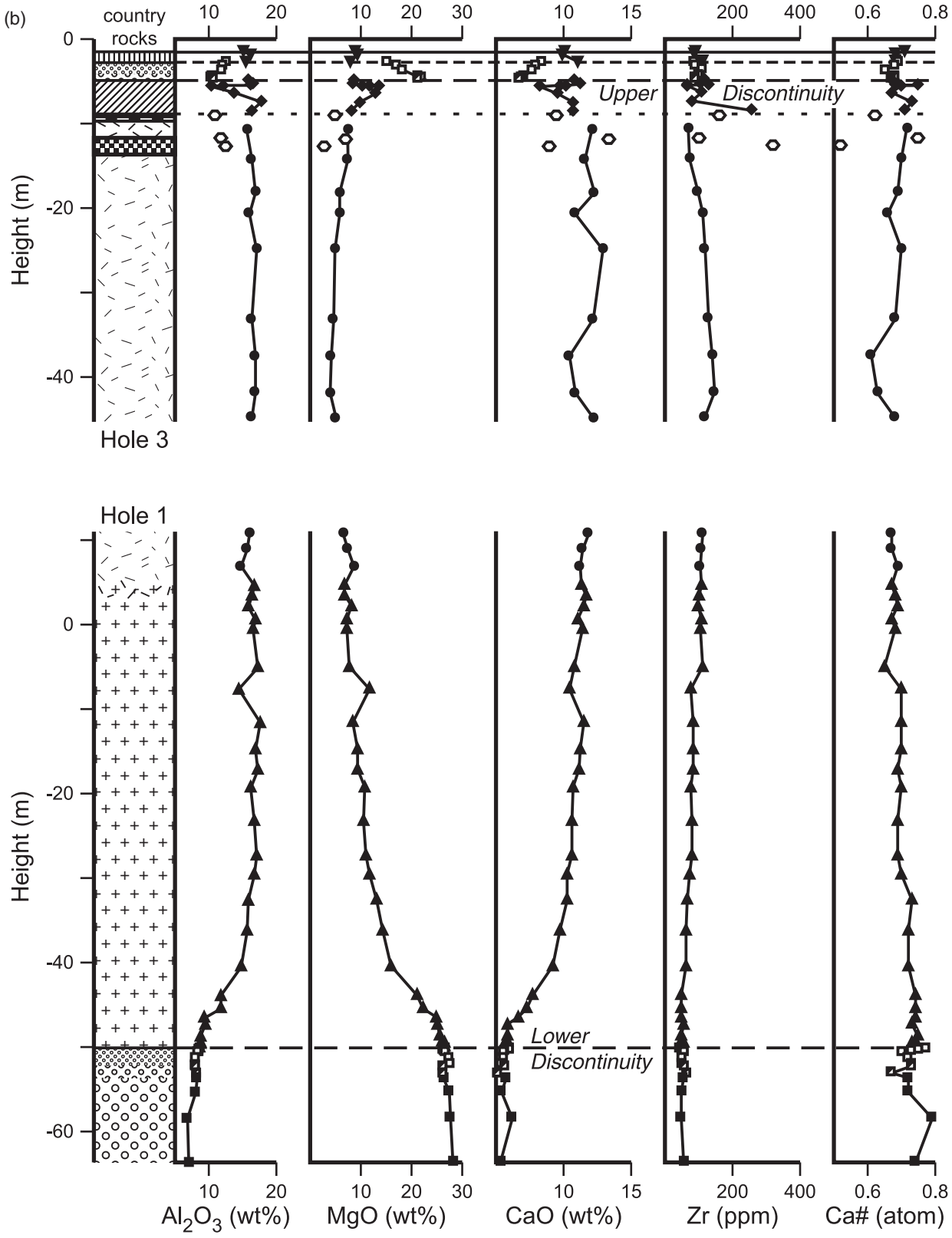

Fig. 5. Continued

the upper and lower cooling surfaces of the sill can be emphasized.

Composite section

The composite section (Figs. 3 and 6a) was originally constructed from the Hole 2 and Hole 3 sections (Figs. 1 and 5) with the +97 m height in the former being equated with the −40 m depth in the latter, as deduced from petrographic and modal data and supported by mineral chemistry (Gibb & Henderson, 1996). Heights, which for the sampled sections are vertical above sea level, were recalculated for the composite section to vertical above the base of the sill and are given in italics, following previous practice (Gibb & Henderson, 1996). We have now used the whole-rock chemistry to refine this model by adjusting the overlapping trends vertically for each element in Hole 3 and Hole 2 until the best visual fits were obtained. For all elements except Sr, this fit was within a few metres of that based on modal and petrographic criteria and the average fit is virtually identical, thus further increasing confidence in the composite section (Fig. 6a). It is evident that no amount of vertical adjustment would produce a reasonable fit for Sr. However, Foland *et al.* (2000) have shown that much of the Sr was introduced during post-solidification alteration of the sill rocks by hydrothermal fluids derived from the country rocks. We therefore discount the mismatch for Sr and indeed will not use Sr for any of the petrogenetic deductions.

Geochemical variations with height

Element distributions with height in the lower three-quarters of the sill are of two main types. In the first, the element concentrations are controlled by the modal amounts of olivine and chrome spinel, the latter being common as inclusions in olivine throughout the picrites and lowermost picrodolerites (Gibb & Henderson, 1996, fig. 3). Chemical parameters exhibiting this type of distribution include MgO, Ni and Cr (not shown). Concentrations increase slightly upward through the olivine teschenites, then across the junction with the picrites (Fig. 6). They continue to increase upwards through the picrites to a maximum before decreasing towards the Lower Discontinuity. Above the discontinuity, the concentrations decrease rapidly upward through the picrodolerites, reaching a relatively constant value in the crinanites. Fe_{Total}, FeO and Mn also exhibit this type of distribution, but with less marked variations in the picrites and smaller decreases through the picrodolerites (Table 1). Mg# [= Mg/(Mg + Fe^{2+}), atomic proportions] also has a similar distribution profile (Fig. 6). [Because variable oxidation effects are likely to have been associated with late- and post-magmatic hydrothermal alteration, we have calculated Mg# taking magmatic Fe^{2+} to be 85% of the total Fe content (Brooks, 1977).]

The second type of element distribution is essentially a mirror image of the first (Figs. 5 and 6a). Elements with these 'mirror image' profiles are mainly those concentrated in plagioclase (Al, Ca, Na, K, Sr), augite (Ca, Ti), iron oxides (Ti, V) and apatite (P, REE), or are incompatible (e.g. Zr, REE, Nb, Th). As the plagioclase/pyroxene ratio changes only slightly throughout the sill (Gibb & Henderson, 1996, fig. 3), these element variations appear to be largely inverse to the olivine content.

The vertical distribution of olivine and compositional variations in olivine (Johnston, 1953; Gibb & Henderson, 1996) and clinopyroxene (Gibb, 1973) are ample proof of the sill's vertical differentiation in terms of Mg#. In addition, throughout the Lower Picrite unit, especially in Hole 2 (Fig. 5a), the Ca# [= Ca/(Ca + Na + K), atomic proportions] has a D-shaped profile, indicating that the unit is slightly more primitive in its centre than at the edges. Above the discontinuity, there is a slight but steady decrease in Ca# up through the picrodolerites and crinanites.

Element distributions through the uppermost part of the sill are essentially the inverse of those in the lower part, again with two types that are mirror images of each other. In the first type (e.g. MgO, Ni, Cr), concentrations are relatively constant through the Upper Olivine Teschenite (Fig. 6b). Across the junction with the Upper Picrite, there is a marked increase that continues down through the picrites to the Upper Discontinuity. Within the GOPd, the profiles reflect the tripartite petrographic subdivision of this unit with its central olivine-rich 'plug' (Foland *et al.*, 2000; Henderson *et al.*, 2000). In the crinanites just below the GOPd, the situation becomes complicated by the presence of pegmatitic horizons. In the highest crinanite, concentrations are similar to those in the Upper Olivine Teschenite, then decrease downwards over ~15–20 m to the lowest values found in the crinanites and remain relatively constant for ~30 m before increasing again.

In the second, 'mirror image'-type of distribution (e.g. Al_2O_3, CaO, Na_2O and the incompatible trace elements), the concentration varies slightly within the Upper Olivine Teschenite then falls sharply across the junction with the Upper Picrite, through which it continues to decrease towards the Upper Discontinuity (Figs. 5b and 6b). A marked increase across the Upper Discontinuity is followed by a decrease into the olivine-rich centre of the GOPd, before another increase into the lower part of this unit. Distribution patterns at the base of the GOPd are a little erratic, possibly reflecting the fact that this part of the unit shows the highest degrees of contamination (Foland *et al.*, 2000). Perhaps significant in this context is Zr, which, in the lowest analysed GOPd, reaches levels exceeded only in the pegmatitic horizons (Fig. 5b).

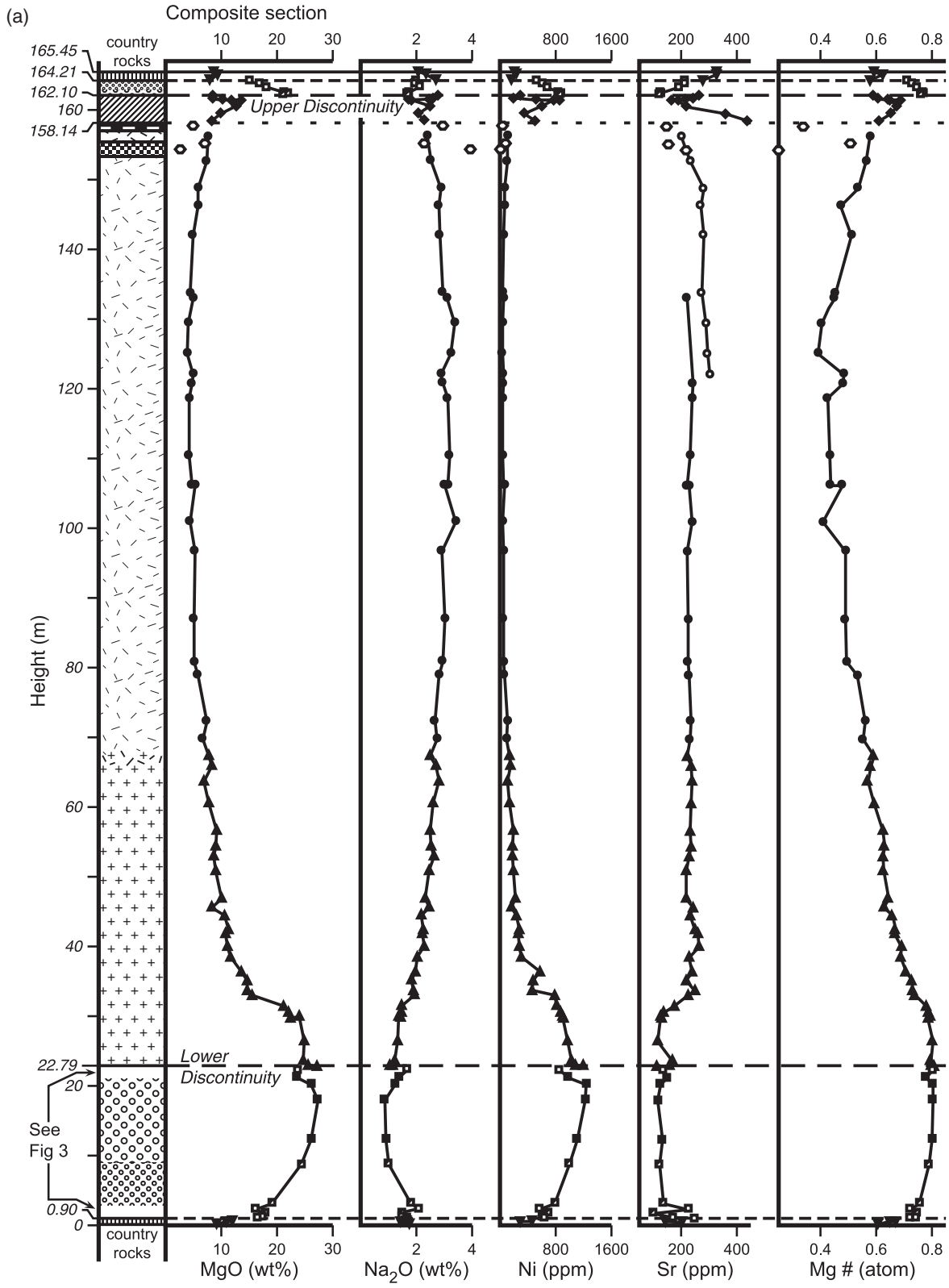

Fig. 6. Vertical variations in selected chemical parameters for (a) the complete composite section with (b) enlargements of the uppermost 16 m and lowermost 5 m. Mg# = Mg/(Mg + 0·85Fe_{total}) (atomic proportions). Symbols and ornaments as in Fig. 2b. Crinanites from the Hole 3 section are shown as open circles on the Sr plot in Fig. 6a to distinguish them from Hole 2 crinanites (see text).

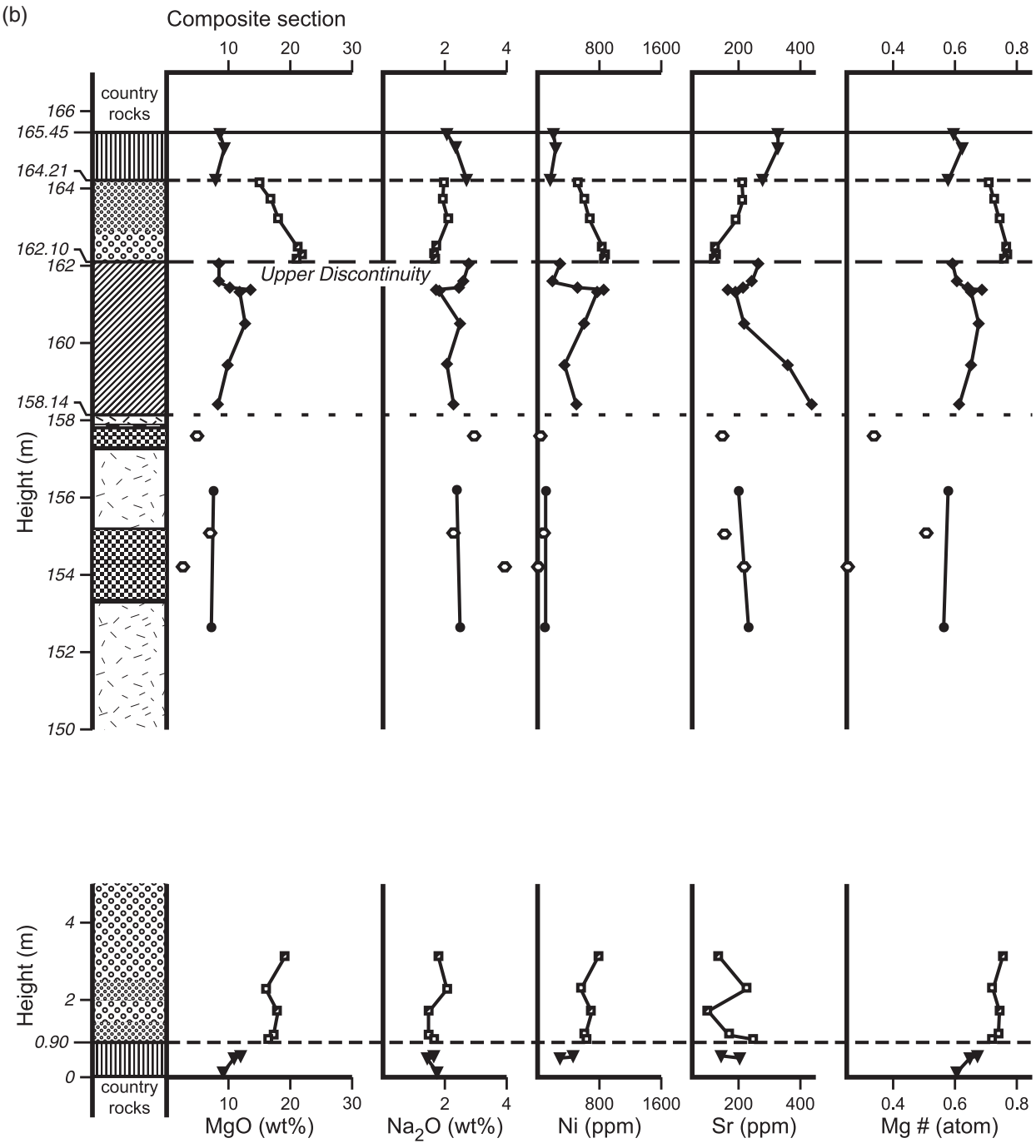

Fig. 6. Continued.

Below the GOPd, concentrations in the uppermost crinanites return to values similar to those in the olivine teschenites (Figs. 5b and 6b) before increasing downward to converge with the concentrations in the crinanites at the top of the Hole 2 section. For most of the incompatible trace elements maximum concentrations occur around the 120 m level in the composite section, where values are typically two to three times those at the top and bottom of the Picrodolerite–crinanite unit.

BOUNDARIES OF INTRUSIVE UNITS

The subdivision of the sill and the consequent multiple intrusion model arose from the recognition of sharp

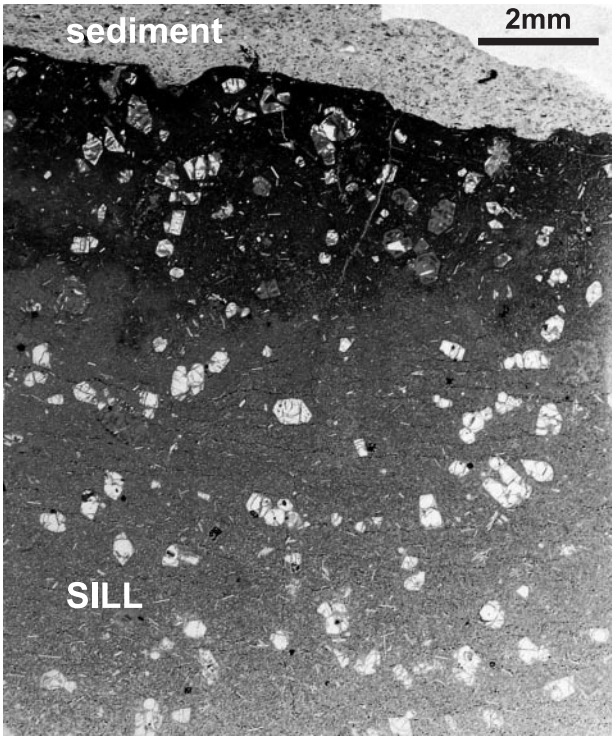

Fig. 7. Thin section (in lane-polarized light) of the upper contact of the sill with sediment showing the distribution of euhedral olivine phenocrysts and plagioclase microphenocrysts (laths) in the chilled margin.

internal boundaries based on field and petrographic evidence, especially changes in modal mineralogy and grain size (Gibb & Henderson, 1989, 1996; Henderson *et al.*, 2000). Such boundaries, at least those across which there are mineralogical changes, should be marked by changes in the whole-rock chemistry. However, where a pulse of magma was emplaced into a hot incompletely crystallized earlier intrusion, rapidly chilled impermeable margins might not have formed. Consequently, there would have been potential for mixing, either of the bulk magmas or of the interstitial liquid from the earlier magma with the new magma. Any such mixing would blur changes in chemistry across the junctions. Indeed, Foland *et al.* (2000) invoked just such a mechanism to account for the variation in isotope chemistry within, and across the lower boundary of, the GOPd unit.

Upper margin of the sill

The upper margin has been sampled and analysed only from Hole 3. The extremely fine-grained marginal rock contains 14% of small euhedral to subhedral phenocrysts of olivine (<0·9 mm long) and sparse microphenocrysts of plagioclase (<0·3 mm long) (Fig. 7). The analysed sample (SC988, Table 1) is 5 cm below the actual contact with the sediments, but is petrographically similar to the marginal rock, albeit slightly less fine-grained.

Corrigan (1982) ascertained the cooling rate through the plagioclase crystallization interval across basaltic dykes by reproducing experimentally the plagioclase grain size. The composition of the upper margin of the sill is similar to Corrigan's "Dyke 1". Applying Corrigan's experimental data to the sill (avoiding obvious phenocrysts) indicates that the rock 1 cm below the contact cooled through the nucleation and growth intervals of the plagioclase at a rate in excess of 10°C/h. Such fast cooling argues against large-scale turbulent convection having occurred in the sill, as the establishment of such convection would greatly reduce the cooling rate at the top of the sill (Huppert & Sparks, 1989). It would be even more inconsistent with a margin formed after melt-back of an original chilled selvedge as a result of increased heat flow from vigorous internal convection in the sill, and we can only interpret this upper margin as having formed by rapid cooling of the intruded magma against relatively cold country rock.

The rapid growth of olivine from quickly cooled basaltic or picritic magmas results in skeletal crystals (Drever & Johnston, 1957). Donaldson (1976) showed experimentally that skeletal olivines grow from a basaltic liquid cooled at rates greater than about 2·7°C/h, while subhedral and granular crystals form at slower cooling rates. The euhedral nature of the olivine phenocrysts in the upper margin of the sill and the absence of skeletal crystals suggest that the phenocrysts formed under cooling rates slower (probably much slower) than 2·7°C/h. Clearly, this is inconsistent with their formation at the same time as the groundmass plagioclase. Latypov (2003*b*) has argued that, as non-skeletal olivine crystals can form at cooling rates up to 2 or 3°C/h, the presence, size and shape of phenocrysts in the chilled margins of intrusions cannot be used to determine whether they formed before or after emplacement. Notwithstanding Latypov's argument, the abundance, size and euhedral habit of the olivine phenocrysts in the upper margin of the sill, together with the fine-grained nature of the groundmass, lead us to conclude that the olivines were present in the magma at the time it chilled against the sediments, i.e. their crystallization pre-dated emplacement. The same is almost certainly true of the plagioclase microphenocrysts.

Hence, while this chilled margin might not represent the bulk composition of the sill, or even of the Olivine Teschenite unit, it does represent the composition of the upper part of the leading edge of the first thin wedge of magma as it propagated along the fracture that was to develop into the sill.

Olivine teschenite–picrite

This boundary is recognized by a sudden downward change to a finer-grained rock accompanied by a more than fourfold increase in modal olivine. The latter is

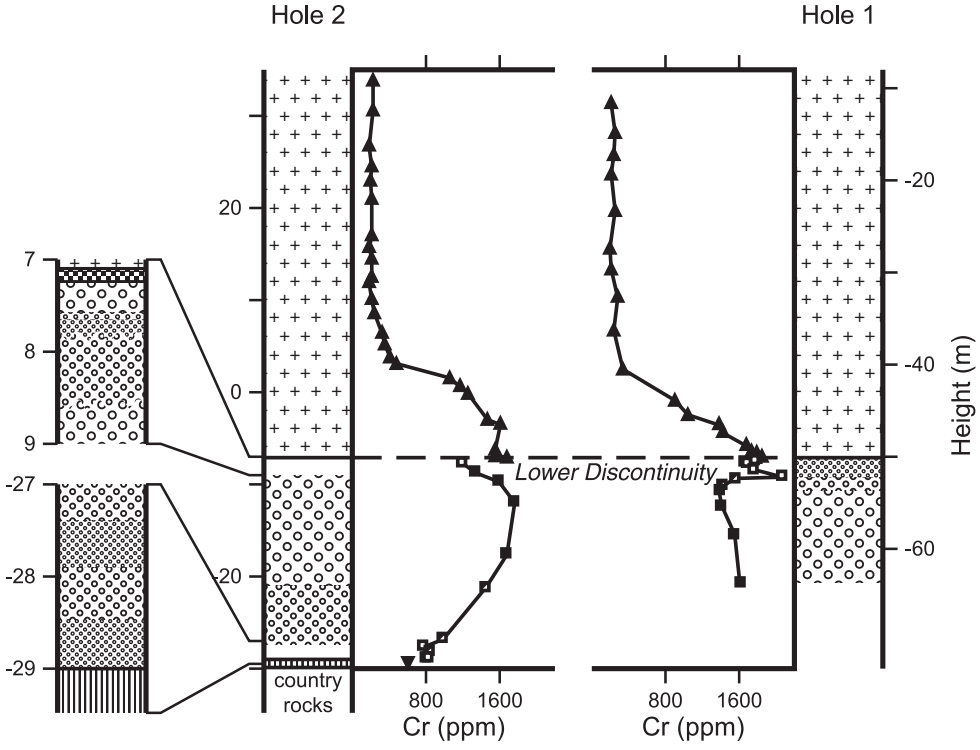

Fig. 8. Distribution of Cr in the lower parts of the Hole 1 and Hole 2 sections.

reflected by substantial increases in MgO, Ni and Mg# (Fig. 6), with smaller rises in total Fe and Cr. There are concomitant decreases in Al_2O_3, CaO (Fig. 5b), SiO_2, Na_2O and the incompatible elements. Chemically, as well as petrographically, this boundary represents a clear break that can be interpreted as a 'reversal' in the sense of a change to a more primitive composition by the intrusion of fresh magma.

Upper discontinuity

In terms of grain size, mineralogy and chemistry, this is the most pronounced break in the sill with medium-feldspar picrite (above) against a very fine-grained facies of the GOPd. Downward across this junction, there are marked increases in Al_2O_3, CaO (Fig. 5b), Na_2O, K_2O, Cr and the incompatible elements with decreases in MgO, Ni and Mg# (Fig. 6). It is difficult to see this as anything other than a mechanical (i.e. intrusive) contact across which there was a change to a less primitive magma. Further, the petrographic characteristics of this boundary suggest the overlying picrite was either solid or a semi-solid crystal mush, and significantly cooler than the GOPd magma when the latter was emplaced (Henderson *et al.*, 2000).

GOPd–crinanite

With relatively subtle grain size changes across this junction, it is the most difficult of the internal boundaries to identify petrographically; however, significant changes between the lowermost GOPd and highest crinanite (Table 1) occur for Cr (3500–260 ppm), Ni (500–125 ppm) and Zr (255–70 ppm). Other clear changes occur in CaO, TiO_2, Co, Cu and Zn. The Sr and Nd isotope evidence is also consistent with a boundary at this position.

Lower discontinuity

The Lower Discontinuity has been described from the north coast of Garbh Eilean (Fig. 1) (Murray, 1954*b*), the SE coast of Garbh Eilean (Murray, 1954*b*; Gibb & Henderson, 1989), the east coast of Eilean an Tighe (Murray, 1954*b*; Gibb & Henderson, 1989) and Drill-holes 1 and 2 (Fig. 1; Gibb & Henderson, 1996). Breaks in modal mineralogy, grain size and texture occur across the discontinuity and marked local variations, especially in the nature of the picrite immediately below it (Fig. 8), might suggest the presence of a transgressive intrusive contact between the Picrodolerite–crinanite and its host Picrite unit.

Whole-rock chemical profiles across the Lower Discontinuity are available from the well-exposed locality on Garbh Eilean (Gibb & Henderson, 1989, fig. 3) and Holes 1 and 2. For ~5–6 m on either side of the Lower Discontinuity in Hole 1, there is a very irregular distribution of Ni and Cu that contrasts with the relatively systematic variation in Hole 2. These anomalously high

concentrations reflect the localized occurrence of pentlandite and chalcopyrite that could have formed by introduction of hydrothermal S-bearing fluids along the discontinuity (Gibb & Henderson, 1996; Henderson *et al.*, 2000).

The contrast between Cr distributions within the picrites immediately below the Lower Discontinuity in Holes 1 and 2 (Fig. 8) may be related to grain size, petrographic and mineralogical differences in the picrites. In Hole 1, the large-feldspar picrite, some 5 m below the discontinuity, grades upwards through medium-feldspar picrite to small-feldspar picrite at the discontinuity, whereas in Hole 2, a similar gradation to small-feldspar picrite occurs but then reverses so large-feldspar picrite reappears below the Lower Discontinuity. Differences in the augite (0·5% Cr_2O_3) and chrome spinel (20–25% Cr_2O_3) contents of the picrite variants are the likely cause of the disparities in the Cr profiles.

Across the Lower Discontinuity (from picrodolerite to picrite) in Hole 2, Gibb & Henderson (1996, fig. 5) recorded a small increase in the Mg# of the olivine (~2%Fo) and a decrease in olivine Ni content. However, no corresponding changes were observed in the compositions of the plagioclase and augite. Gibb (1973) and Gibb & Henderson (1996) attributed these features to post-intrusive equilibration of interstitial liquids across the discontinuity while both picrite and picrodolerite were crystal mushes.

We conclude that changes in chemical composition across the Lower Discontinuity confirm the field and petrographic evidence that it is an intrusive contact (possibly transgressive) formed by the emplacement of the Picrodolerite–crinanite unit into the earlier Picrite.

Picrite–olivine teschenite

Petrographic identification of this boundary, which is recorded only from Hole 2 and Drill-hole DJ2 (Fig. 1), is hampered by the increasing alteration of the rock towards the bottom of the sill. However, it is more clearly defined by the breaks in element concentrations and element ratio profiles. These breaks are essentially inverted versions of those across the olivine teschenite–picrite boundary just below the top of the sill (Figs. 5 and 6).

Lower margin of the sill

The lower margin of the sill has been studied from isolated, poorly exposed outcrops along the north coast of Garbh Eilean (Drever & Johnston, 1959), from Drill-hole DJ2 (Drever & Johnston, 1965) and from our Hole 2. The rock from the north coast, described by Drever & Johnston as the lower margin, consists of about 15% of small, mainly euhedral or subhedral, phenocrysts of olivine and sporadic microphenocrysts of plagioclase in a very fine-grained groundmass. It appears to be almost identical to the upper margin of the sill described above [cf. Fig. 7 and plate XVI-D of Drever & Johnston (1959)]. Unfortunately, no chemical analysis of this rock was given. The lowermost 1·3 m of the sill recovered from Drill-hole DJ2 was referred to by Drever & Johnston (1965) as "fine-grained olivine teschenite". Close to the lower margin of the sill, the rock is very heavily altered but was described as "comparable with ... the lower contact ... at the north end of Garbh Eilean". This hydrothermal alteration can be attributed to the activity of convectively circulating, heated groundwater, initially trapped beneath the sill, gaining access to the lower reaches of the sill through contraction fractures formed during post-solidification cooling (Gibb & Henderson, 1978, 1996; Dickin *et al.*, 1984).

The lowest sill sample analysed (SC770) is from 15 cm above the contact where the alteration is less severe. Compositionally SC770 is almost indistinguishable from SC988 just below the upper margin of the sill and any differences are attributable to post-solidification hydrothermal alteration. Thus, the chemistry is consistent with both the upper and lower margins of the sill being formed by the rapid chilling of the leading portion of the first batch of magma intruded into the sill.

MULTIPLE INTRUSION MODEL

The occurrence of paired (top and bottom), inverted breaks in the chemical profiles and the coincidence of these with unit boundaries identified from field and petrographic observations is unequivocal evidence of multiple intrusion (Fig. 4). Further support comes from the chemical coherence of the now separated parts of the earliest intrusive units. This is best seen by restoring the chemical profiles of the sill to what they would have been before the third magma was emplaced to form the Picrodolerite–crinanite unit, i.e. removing everything between the Upper and Lower Discontinuities (Fig. 9). For all modal, mineralogical and chemical parameters, the fit of the internally differentiated Upper and Lower Picrite units is striking. These correspondences are all the more remarkable as (a) the two sections being fitted together are ~400 m apart laterally, and (b) the subsequent intrusion of the crinanitic magma may have been slightly transgressive with respect to the picrite. The restored fits are equally good with respect to Sr and Nd isotope ratios (Foland *et al.*, 2000, figs 4 and 7). Further, this suggests that very little of the picrite was displaced or swept away by the subsequent intrusions.

Going back one stage further to before the intrusion of the Picrite unit and attempting a similar re-fit for the Upper and Lower Olivine Teschenites does not work quite so well. It appears that some of the original

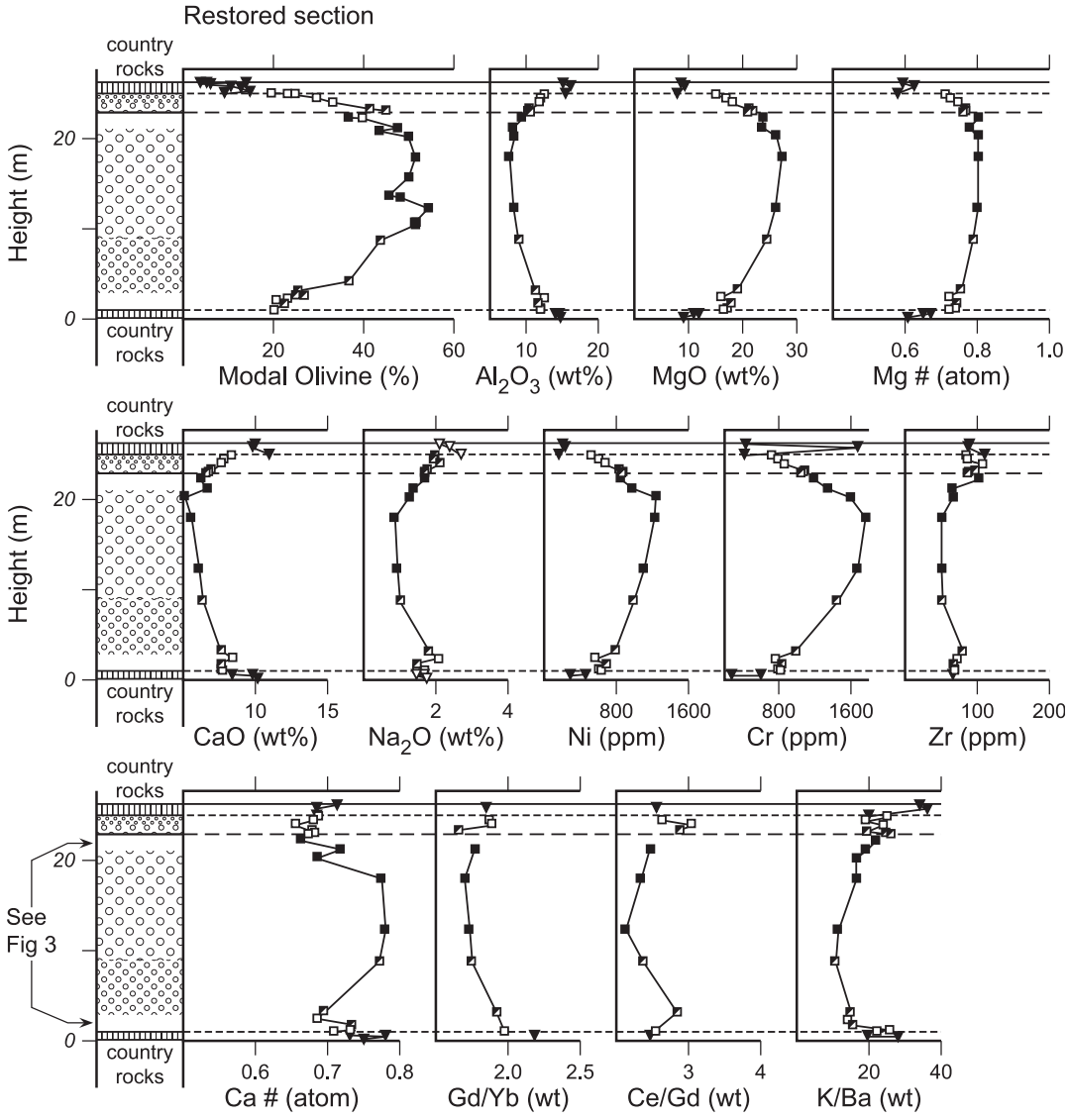

Fig. 9. Variations in modal olivine content and selected chemical parameters for a vertical section through the sill restored to its state before emplacement of the Picrodolerite–crinanite unit. Symbols and ornaments as in Fig. 2b.

teschenite intrusion might have been removed during the emplacement of the Picrite.

OVERALL CHEMICAL VARIATIONS IN THE SILL

We do not present CIPW normative data for the analysed samples; however, it is worth noting that most of the sill rocks are only slightly silica-undersaturated, with about 3% *ne* in the norm. The topmost olivine teschenite (SC988, Table 1) and the lowest two picrites analysed (SC758, SC760) have ~3% *hy* and rocks from the Lower Olivine Teschenite (SC765L, SC770) have ~11% *hy*. All of these *hy*-normative rocks exhibit extensive hydrothermal alteration and the inference is that their major element compositions were disturbed by the post-magmatic processes (Gibb & Henderson, 1996; Foland *et al.*, 2000). The GOPd unit is notably heterogeneous with some rocks (e.g. SC1040, SC1060T) having >10% *hy* but lacking obvious signs of hydrothermal alteration. In these cases, the suggestion is that their *hy* content is a magmatic feature.

Plots of whole-rock major and trace element data against wt % MgO as a differentiation index (Fig. 10) show the overall variations within the sill. The picrites and picrodolerites define a tight linear trend along an olivine control line towards Fo_{83}, the coexisting olivine composition (see arrows in Fig. 10). The picrodolerites with the lowest MgO contents overlap with the

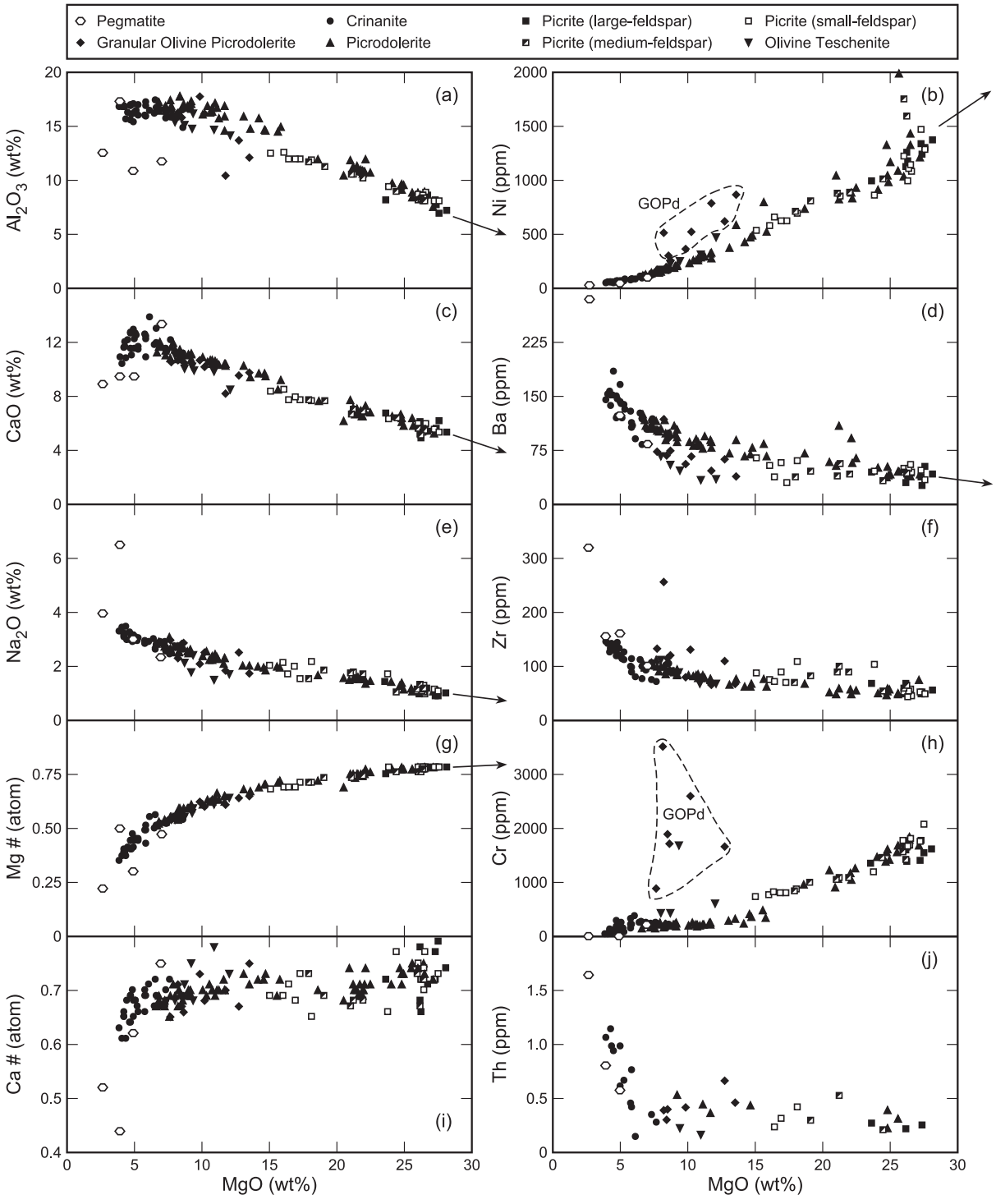

Fig. 10. Whole-rock compositional variations of the sill rocks with MgO (wt %) content. The fields occupied by the GOPds are outlined in (b) and (h). Arrows point to Fo_{83}. Symbols (top) are as in Fig. 2b.

compositional field of the crinanites. The analysed pegmatites have markedly lower Al_2O_3 contents than the crinanites because of their high contents of augite and Ti-magnetite. The olivine teschenites tend to be slightly less aluminous than picrodolerites with similar MgO contents. CaO and Na_2O (Fig. 10c and e) exhibit similar trends along olivine-control lines. Mg# (Fig. 10g) shows a smooth trend with a steeper decrease below ~15% MgO,

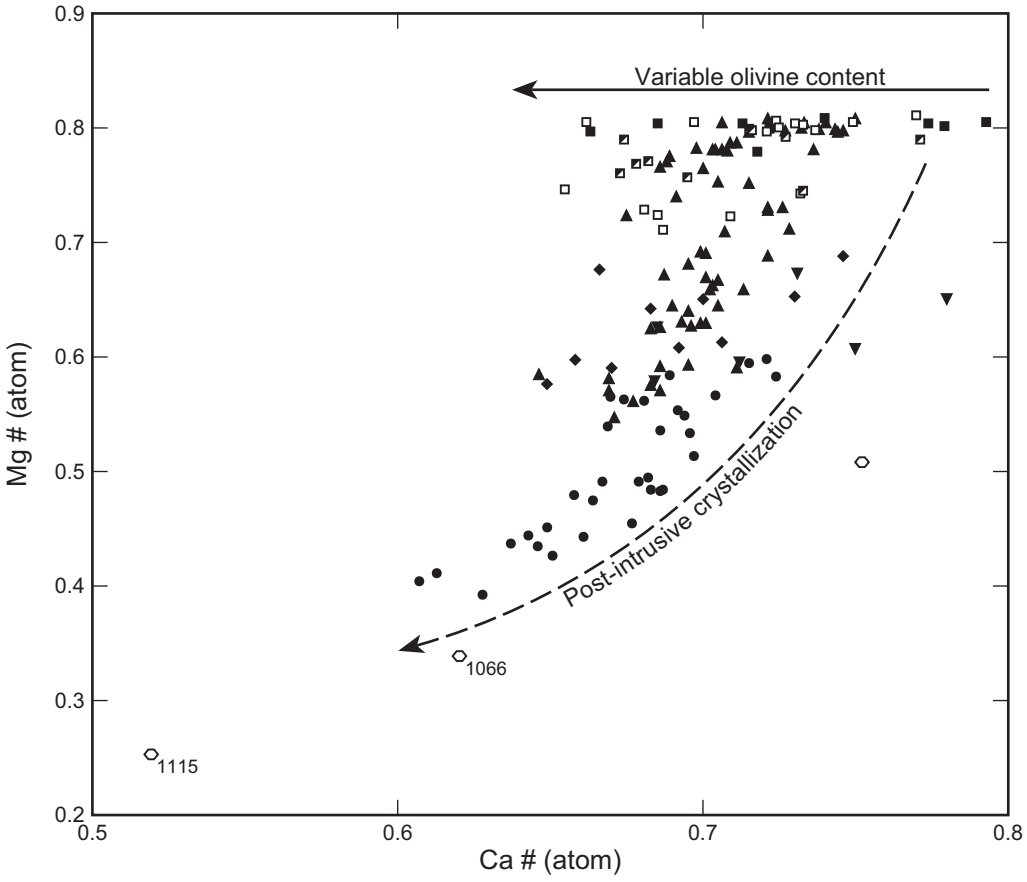

Fig. 11. Plot of Mg# against Ca# for the analysed sill rocks. The arrows show the directions (but not positions) of the indicated processes. SC1066 and SC1115 are two of the pegmatitic specimens referred to in the text. Symbols as in Figs. 2b and 10.

reflecting the increased Fe enrichment in the olivine teschenites, GOPds and especially the more evolved picrodolerites, crinanites and pegmatites. By contrast, Ca# (Fig. 10i) shows only a small decrease until the crinanites and pegmatites. This reflects the fact that albite enrichment in plagioclase became dominant only during the latest stages of sill solidification.

As expected, Ni decreases sympathetically with MgO (Fig. 10b), but is somewhat variable at the MgO-rich end of the trend because of the occurrence of Ni-bearing sulphides in picrodolerites and picrites close to the Lower Discontinuity. The GOPds lie significantly above the trend and the same is true for Cr (Fig. 10h), where the data are even more scattered. This is because of the variable contents of Cr-rich spinel in the GOPds. Both large ion lithophile (e.g. Ba, Th: Fig. 10d and j) and high field strength (e.g. Zr: Fig. 10f) incompatible element contents increase as MgO decreases, with the strongest enrichment in the crinanites and pegmatites.

A plot of Mg# against Ca# (Fig. 11) allows the effects of variation in the content of (introduced) olivine and post-intrusive fractionation of the liquid to be distinguished. All the large-feldspar picrites and some of the medium- and small-feldspar picrites have Mg#s around 0·80, but Ca# varies from 0·79 to 0·66. The olivine in this group of rocks has a composition close to Fo_{83} (Gibb & Henderson, 1996) and the relatively constant Mg# indicates that this olivine (which was mainly present as crystals at the time of emplacement) is the dominant ferromagnesian mineral. [A table of mineral compositions for the analysed rocks (Electronic Appendix 1 is available at http://www.petrology.oupjournals.org).] On the other hand, the Ca, alkalis, Al, etc. are contributed largely by minerals that crystallized *in situ* from the co-existing liquid phase; the range shown by Ca# reveals that the composition of this liquid was variable through the Picrite unit with the less evolved rocks (higher Ca#) being located in the centre of the unit. This could reflect an original feature of the intruded magma or subsequent migration of interstitial liquid during *in situ* differentiation of the Picrite, or possibly both (see later). The remaining medium- and small-feldspar picrites form a second group with Mg#s between 0·70 and 0·78 and Ca# varying from 0·65 to 0·73. These latter picrites are more evolved than the first group and reflect their lower contents of suspended olivine crystals. It is significant that

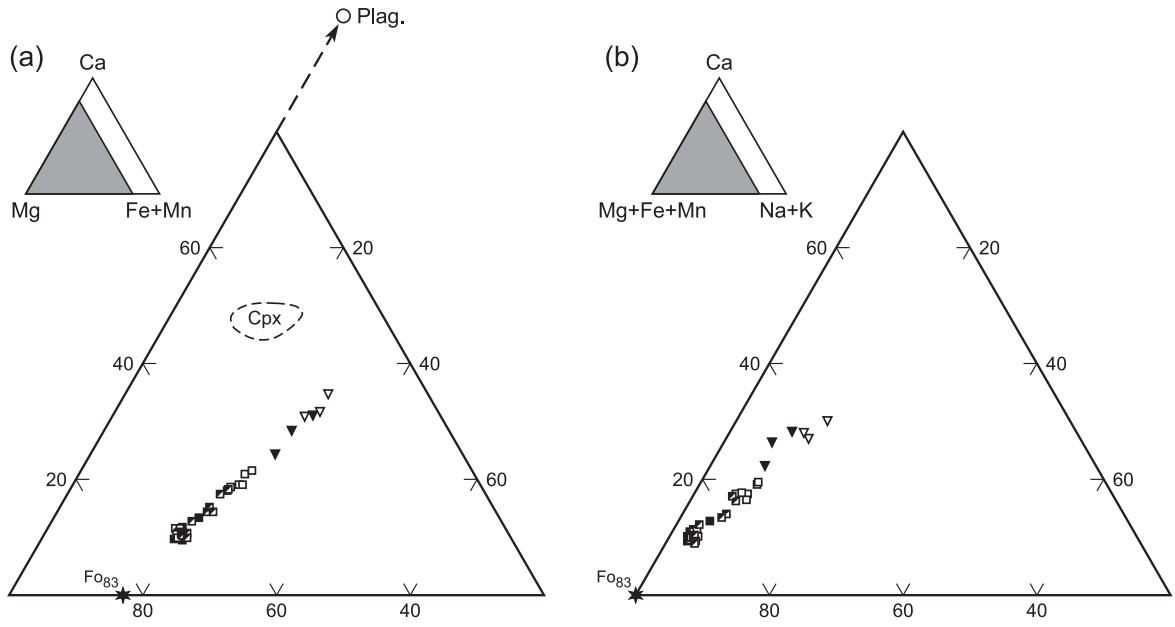

Fig. 12. Atomic proportions triangular variation diagrams for olivine teschenites and picrites. (a) Ca–Mg–(Fe + Mn); Cpx, field of clinopyroxenes (from Gibb & Henderson, 1996, fig. 7). (b) Ca–(Mg + Fe + Mn)–(Na + K). Symbols as in Figs. 2b and 10 but with analyses from the Upper Olivine Teschenite unit shown as open symbols (see text). The star symbol indicates the position of olivine (Fo_{83}).

all the medium- and small-feldspar picrites in the first group are from just below the Lower Discontinuity, whereas those in the second group are from the more marginal parts of the unit.

The more olivine-rich picrodolerites have Mg#s between 0·73 and 0·80, with Ca#s between 0·68 and 0·74, and define a trend with a gentle positive slope, indicating that some *in situ* fractionation was superimposed on the physical redistribution of olivine. The remaining picrodolerites from higher in the unit have Mg#s from 0·54 to 0·73 and Ca#s from 0·65 to 0·72, defining a steeper trend representative of a stronger crystal–liquid fractionation with less of a contribution from olivine accumulation. Most of the crinanites lie on a continuation of this trend to lower Mg#s with a faster decrease in Ca#. Two of the more "crinanitic" pegmatites—SC1066 and SC1115 (see Table 1 for locations of numbered specimens)—extend the trend to the most-evolved rock compositions analysed.

Most of the olivine teschenites in Fig. 11 overlap with the more evolved picrodolerites but two from the heavily altered bottom part of the sill have anomalously high Ca#s as a consequence of the hydrothermal leaching of alkalis.

DIFFERENTIATION WITHIN UNITS

The fractionation trends are best shown in ternary chemical variation diagrams plotted in atomic proportions rather than wt %, making it straightforward to locate and define the effects of the various minerals from their end-member stoichiometries.

Olivine teschenite

On a Ca–Mg–(Fe + Mn) diagram (Fig. 12a), the Upper and Lower Olivine Teschenites define an approximately linear trend that is consistent with evolution through fractionation of olivine ~Fo_{83} (the composition of the most Mg-rich olivine found in the rocks). The lack of displacements towards the compositions of the plagioclase or clinopyroxene in these rocks (Fig. 12a) indicates that these minerals were not significant at this stage of the sill formation. There is slightly more scatter in terms of Ca–(Mg + Fe + Mn)–(Na + K) in Fig. 12b, with small variable displacements towards the Na + K apex reflecting the presence of analcime in the hydrothermally altered marginal rocks.

The normalized REE patterns for the Upper and Lower Teschenites (Fig. 13f) are sub-parallel and are characterized by a hump-shaped pattern indicating enrichment in the middle REE relative to the HREE, and a slight enrichment in LREE relative to the HREE. There appear to be small positive Eu anomalies superimposed on the pattern. The Upper Olivine Teschenite (e.g. SC1000) has higher concentrations of REE (Fig. 13f), and incompatible trace elements (Fig. 14f) than the Lower Olivine Teschenite (e.g. SC765L). This may be largely due to the higher olivine content in the latter. The parallel nature of the trends in Figs 13f and 14f reflects the immobility of the REE and most incompatible

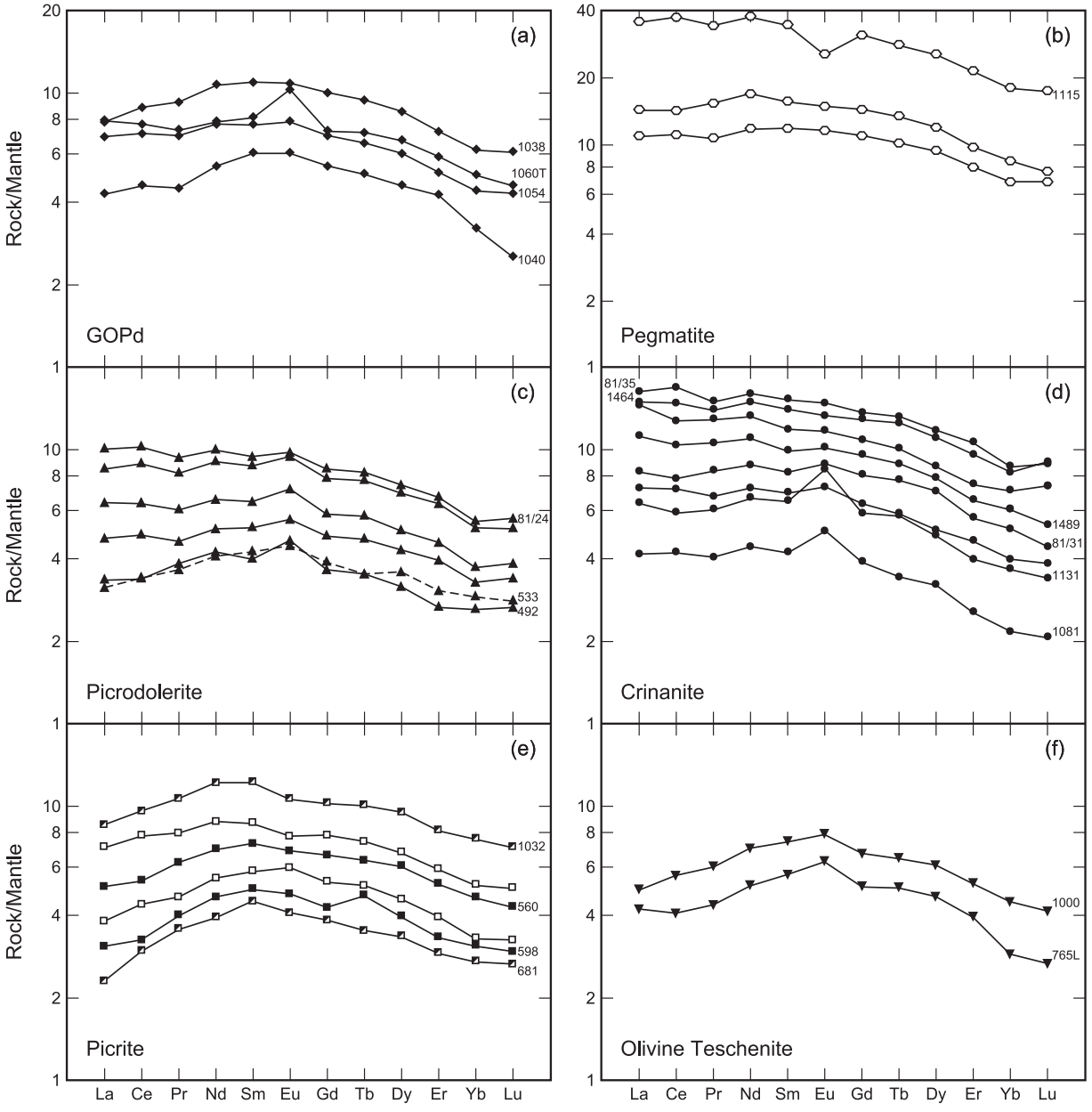

Fig. 13. Representative REE diagrams for the different rock types (a)–(f) normalized to the mantle composition of McDonough & Sun (1995). Specimen numbers are shown only for samples mentioned in the text (see Table 1 for locations of samples). Symbols as in Figs. 2b and 10.

elements during hydrothermal alteration, which was greater in the Lower than the Upper Olivine Teschenite. The incompatible element diagram (Fig. 14f) indicates depletions in Th and Nb and a characteristic depletion in P. There also appear to be enrichments in Ba, Rb and K but little significance is attached to these, as Ba, Rb and K may not have remained completely immobile during the hydrothermal stage that affected the Sr distribution in the sill (although there is no evidence of this).

There can be little doubt that the olivine teschenite was emplaced as a suspension of ~14% olivine phenocrysts (often with small inclusions of Cr-spinel) and sparse plagioclase microphenocrysts (Fig. 7). Variations in modal mineralogy and whole-rock chemistry suggest that the existing Upper and Lower Olivine Teschenite units represent only part of the original olivine teschenite intrusion, the missing central part having been swept away by the subsequent intrusion of the picrite.

Picrite

The picrites define a strong linear olivine (Fo_{83}) control trend in Fig. 12 extending from the olivine-rich,

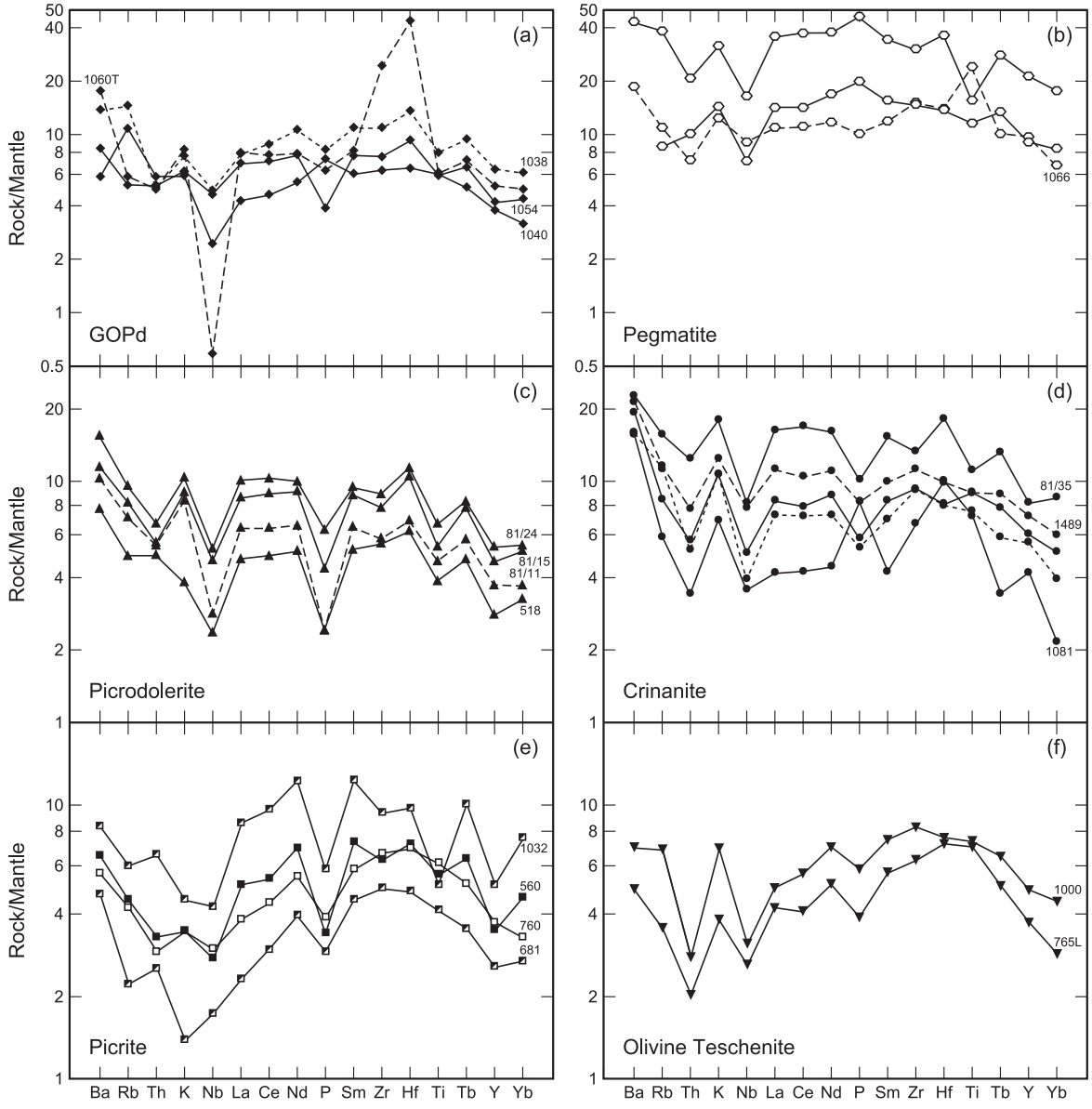

Fig. 14. Representative incompatible trace element diagrams for the different rock types (a)–(f) normalized to the mantle composition of McDonough & Sun (1995). Sr, which normally plots between Ce and Nd, has been omitted because of its largely hydrothermal origin and low temperature mobility throughout the sill. Symbols as in Figs. 2b and 10. Samples plotted are not necessarily the same as in Fig. 13, to avoid confusing overlap.

large-feldspar picrites through medium-feldspar picrites to the small-feldspar picrites found near the top and bottom of the Upper and Lower Picrite units. However, a significant number of medium- and small-feldspar picrites plot at the high-Mg end of the trend along with the large-feldspar picrites. These are the picrites from the internal part of the unit and contrast with the first group of similar grain size, but olivine-poorer, picrites from closer to the margins. Clearly, position in the sill is more relevant than petrographic type to the chemistry of the rock. The fact that the picrites plot on tight linear trends with no displacements towards plagioclase or clinopyroxene (Fig. 12a) shows that these phases were still not significant at this stage of the evolution. The magma intruded to form the Picrite unit was thus a suspension of olivine crystals ($\sim Fo_{83}$) in a liquid of slightly variable composition. The liquid composition must lie on a continuation of the picrite trend towards the Ca–(Fe + Mn) side of Fig. 12a and towards the Ca–(Na + K) side of Fig. 12b. The projected trend would intersect the Ca–(Na + K) side of Fig. 12b at about 75:25, suggesting that the liquid contained feldspathic components with a

composition of $\sim An_{75}$. The composition of the liquid is deduced in a later section.

The normalized REE patterns for all picrites (Fig. 13e) have the same characteristic hump shape as those for the olivine teschenites and, although most exhibit a small overall LREE enrichment (La/Lu), e.g. SC1032, not all do, e.g. SC681. Samples from the Upper Picrite generally have higher REE concentrations than those from the Lower Picrite, with those from the central, most olivine-rich part of the unit (e.g. SC598 and SC681) having the lowest REE contents of all. The tendency for samples from the Upper Picrite to exhibit higher LREE/HREE ratios than those from the Lower Picrite could be related to the suggestion (Foland *et al.*, 2000) that some of the interstitial liquid from the upper parts of the Picrodolerite–crinanite unit migrated up into the overlying Upper Picrite prior to intrusion of the GOPd. The incompatible trace element patterns (Fig. 14e) also show higher concentrations in the Upper Picrite than in the Lower Picrite, consistent with this suggestion.

The D-shaped olivine distribution (Figs. 3 and 9) in the Picrite arose during emplacement as a result of fluid-mechanical redistribution of the suspended crystals (by flow differentiation) or through temporal variations in the phenocryst content of the magma, and probably both. The distribution was not modified significantly by any post-intrusive processes, such as gravity settling or thermal convection (Gibb & Henderson, 1992). However, while introduced olivine content is the dominant factor controlling the differentiation of the Picrite unit, the similarly D-shaped profile for Ca# (Fig. 9) and the compositional profile for the clinopyroxenes (Henderson *et. al.*, 2000), which crystallized *in situ*, confirm that the centre of the unit is more primitive than the margins in other respects. This is shown well by K/Ba (Fig. 9), which varies from more primitive (lower) values in the centre to more evolved (higher) values at the margins, probably controlled by fractionation of plagioclase in which Ba is incorporated preferentially to K (Berlin & Henderson, 1969; Philpotts & Schnetzler, 1970). The variation in the shape of the REE patterns also reflects the position in the Picrite unit, as shown by the symmetrical variation of Gd/Yb and Ce/Gd with stratigraphic height (Fig. 9). Enrichments of LREE relative to MREE and MREE relative to HREE are features of the more evolved crinanites and pegmatites (Fig. 13b and d). We interpret the slightly more evolved nature of the margins of the Picrite unit as evidence of temporal variation, not only in the phenocryst content, but in the liquid composition of the magma during emplacement of the picrite. This was possibly a result of tapping less and less evolved regions of a zoned parental magma body as magma withdrawal progressed, combined with decreasing crystallization in the feeder system as flow-through increased.

Henderson *et al.* (2000) suggested that the enrichment of K_2O in plagioclase and kaersutite in the Upper Picrite relative to that in the Lower Picrite might be due to evolved, volatile-rich, silicate liquids from the crinanites, related to formation of the pegmatite horizons (which contain significant K_2O), migrating upwards into the still-hot overlying picrites, prior to emplacement of the intervening GOPd. A less likely possibility was influx of alkali-rich aqueous fluids from the overlying sediments (cf. Sr). The fact that the Upper Picrite also tends to have elevated concentrations of LIL and HFS incompatible trace elements favours the former mechanism.

Picrodolerite–crinanite

In Fig. 15a, the picrodolerites define a fairly tight trend but the crinanites, lying on an extension of this trend, show more scatter. This is largely a sampling effect. Unlike the olivine, plagioclase and augite in the picrodolerite, which are small to medium in size and fairly evenly distributed, the augitic clinopyroxenes in the crinanites tend to occur as very large (up to 3 cm) ophitic crystals separated by plagioclase-rich areas. This tendency increases upwards from the picrodolerite–crinanite transition and the olivines become larger and sub-ophitic (Gibb & Henderson, 1996). As the amounts of material available for analysis were often limited by the diameter of the core (22 mm), the distribution of large crystals within the sample could be responsible for most of the scatter seen in Fig. 15 and explain why it is greater in Fig. 15a (in which the clinopyroxenes plot above and well off the trend) than in Fig. 15b.

The underlying cause of the variation through most of the picrodolerites (Fig. 15) is the differential distribution of olivine ($\sim Fo_{83}$ = the composition found in the picrites and lowermost picrodolerites). In the higher picrodolerites and crinanites, however, there is a slight but definite curvature to the trend of Fe enrichment (Fig. 15a) that reflects the upward-increasing Fe contents of the olivines and pyroxenes in this part of the sill (Johnston, 1953; Gibb, 1973; Gibb & Henderson, 1996). The less curved nature of the trend in Fig. 15b indicates that this Fe enrichment is accompanied by alkali enrichment, as reflected in the compositions and distributions of the feldspars and analcime (Gibb & Henderson, 1996). (For mineral compositions, see Electronic Appendix 1.) The most evolved crinanites plotted in Fig. 15 are SC1464 and SC1397 from between 125 m and 130 m in the composite section (Fig. 6). This is only slightly lower stratigraphically than the levels with the most evolved and strongly zoned minerals (Johnston, 1953; Gibb, 1973; Gibb & Henderson, 1996), suggesting that the upward and downward solidifying parts of the crinanite met between 125 and 135 m.

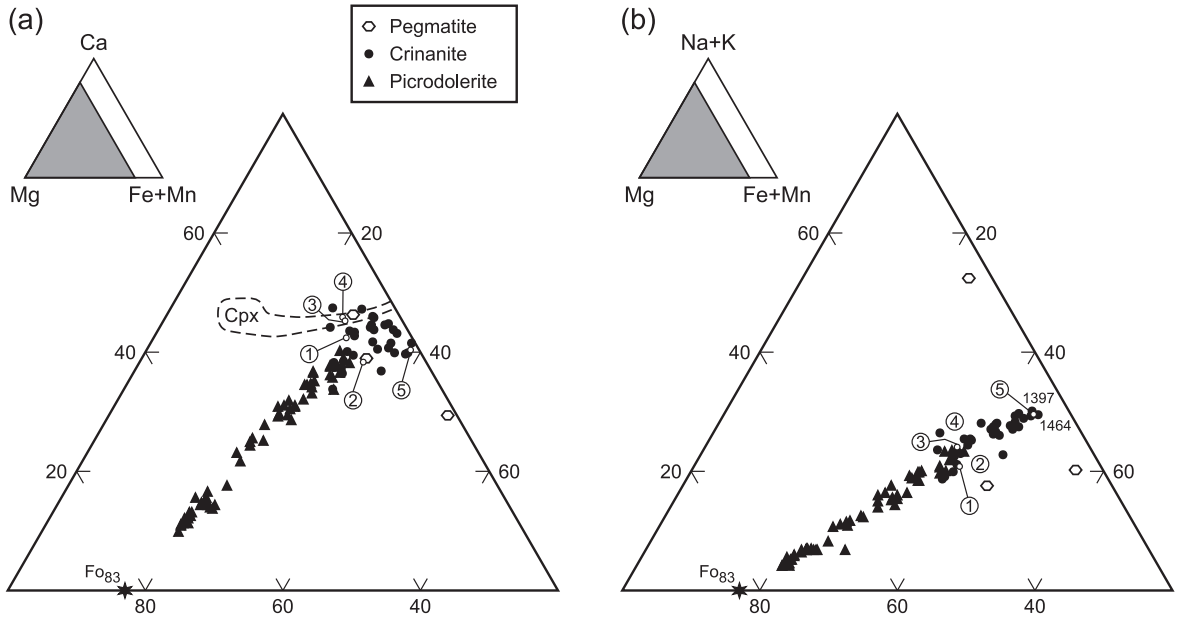

Fig. 15. Atomic proportions triangular variation diagrams for picrodolerites, crinanites and pegmatites. (a) Ca–Mg–(Fe + Mn); Cpx, field of clinopyroxenes (from Gibb & Henderson, 1996, fig. 7); numbered circles are the compositions of calculated parent liquids (Table 2) as follows: 1, PicrPL; 2, OTPL; 3, PdolPL1; 4, PdolPL2; 5, Evolved crinanite. (b) (Na + K)–Mg–(Fe + Mn). Symbols (top) as in Figs. 2b and 10. The star symbol indicates the position of olivine (Fo_{83}).

Three pegmatite samples from near the top of the Picrodolerite–crinanite lie off the main trends for the picrodolerites and crinanites by varying amounts related to their magnetite, plagioclase and analcime contents. These rocks crystallized from Si, Fe, Na, K and volatile enriched liquids derived from the evolving crinanites; however, the location of the pegmatitic horizons so near the top of the Picrodolerite–crinanite unit makes it improbable that they represent a 'sandwich horizon' in the orthodox sense (this occurs ~25 m lower—see above). Rather, it suggests that the evolved, water-rich melts migrated upwards, possibly due to compaction, either to rupture and intrude a semi-rigid, partly crystalline network (Philpotts & Carroll, 1996; Philpotts *et al.*, 1999) or to percolate into gravity-induced tears in the unconsolidated mush of the downward-crystallizing solidification-front (Marsh, 1996). These processes arise from the high compressive strength and high permeability of crystal networks in partly solidified basaltic magmas. Furthermore, the experimental work of Philpotts & Carroll (1996) suggests that the host crinanite was probably not more than 40% crystallized when the pegmatites were emplaced, at which stage much of the underlying part of the unit was still largely liquid.

The picrodolerites from the bottom of the unit (e.g. SC492 and SC533) have the lowest REE contents of all the picrodolerites and crinanites (Fig. 13c and d), resulting from their high olivine contents, and have hump-shaped REE profiles similar to the underlying picrites (Fig. 13e). These picrodolerites also exhibit small positive Eu anomalies. Picrodolerites from higher in the sill show increasing REE abundances upwards, with a progressive change in their profiles towards flatter LREE (La–Sm) patterns and less pronounced Eu anomalies, e.g. S81/24. The crinanites immediately above the picrodolerites (e.g. S81/31) continue this trend up to S81/35 (101 m) and SC1464 (125 m), with increasing LREE enrichment. Above this, the trends reverse through flatter LREE profiles and lower REE contents with little or no Eu anomaly (SC1489) to REE profiles and contents similar to the lower picrodolerites but with even more pronounced positive Eu anomalies, e.g. SC1131 and SC1081 at the 156 m level (Fig. 13d).

Two pegmatites (Fig. 13b) have REE profiles similar to the more evolved crinanites (flat LREE patterns and no Eu anomalies), while the third, SC1115, is more evolved than any of the crinanites with a marked negative Eu anomaly; this is the only analysed sample from the sill that shows the effects of plagioclase fractionation.

Like the REE, the concentrations of incompatible trace elements in the Picrodolerite–crinanite unit (Fig. 14c and d) increase upwards from the lowest picrodolerites [SC533 (not shown) and SC518] to S81/35 and SC1464 before decreasing again towards the highest analysed crinanite (SC1081). Most show depletions in Th and Nb (relative to Ba, Rb and K—see above) and P but some, e.g. SC518, are not depleted in Th while

others have a peak at P instead of the characteristic depletion, e.g. SC1081. The pegmatites have the highest incompatible element concentrations in the sill with similar patterns to the crinanites (Fig. 14b) but without strong P depletions. SC1066 has a positive Ti anomaly consistent with its high content of magnetite.

The variations in incompatible element and REE contents within the Picrodolerite–crinanite unit are greater than can be accounted for by the dilution effect of olivine distribution. We interpret these, accompanied by LREE enrichment, and the distributions of K and Eu anomalies as indicative of an internal differentiation process within the unit. This must have involved modest inward displacement of evolving interstitial liquid that reached a maximum around the 125–135 m level in the sill, with some of the most evolved liquids migrating (mainly upwards) to form the pegmatitic horizons as described above.

The "crinanitic" magma (Foland *et al.*, 2000) that gave rise to this unit was intruded with ~10% olivine and ~1·5% plagioclase crystals in suspension (based on average modal phenocryst data). In contrast to the D-shaped olivine distributions in the Picrite and GOPd units, which were more or less unaffected by post-intrusive settling, the suspended olivines in the Picrodolerite–crinanite unit settled effectively through the liquid and probably continued to grow as they did so. The settling was most efficient for the larger, individual crystals and less so for those aggregated with plagioclase phenocrysts into radiating clusters. Probably the only introduced olivines not to settle into the picrodolerite were those in the uppermost crinanite that became trapped in the downward migrating "capture front" (Marsh, 1996) and some very small crystals that remained suspended in the crinanite. The latter would have acted as nucleii for the subsequent growth of the large zoned ophitic olivines that developed through *in situ* cotectic crystallization with plagioclase. The ranges of zoning present in all the main minerals indicate that crystallization throughout most of the unit took place under conditions of near-perfect local fractionation (Gibb & Henderson, 1996). That gravity settling of the introduced crystals was effective in this unit but not (or much less so) in the earlier Picrite and Olivine Teschenite units must be a consequence of the larger crystal size, lower concentration of suspended crystals and longer cooling time of the Picrodolerite–crinanite unit.

Granular Olivine Picrodolerite

On variation diagrams such as Figs. 10 and 11, the GOPd samples form a more evolved group than the picrites, fall around the middle of the picrodolerite trend, and often coincide almost exactly with the olivine teschenites. Two sub-sets can be distinguished in

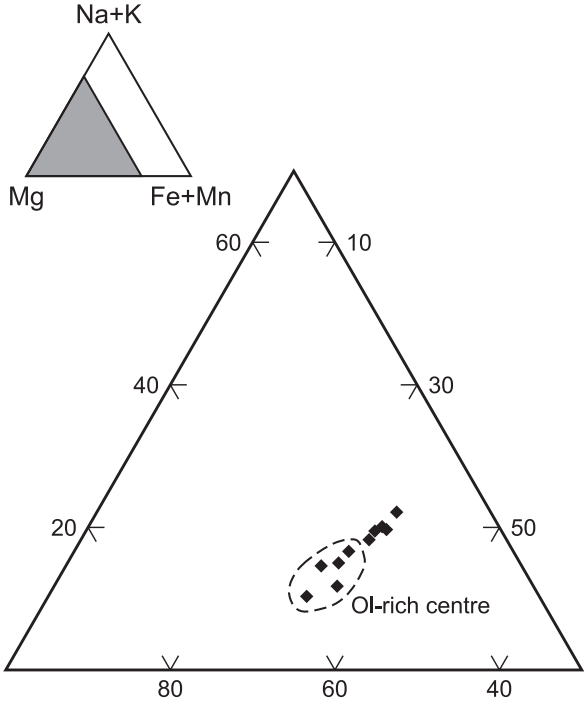

Fig. 16. Atomic proportions triangular variation diagram, (Na + K)–Mg–(Fe + Mn), for GOPd. The field of samples from the olivine-rich central part of the unit is indicated.

Fig. 16—one comprising GOPds from the olivine-rich central section of the unit and the other consisting of samples above and below it. The linear trend defined by the GOPds marks the control exerted by olivine distribution, but it suggests an olivine composition between Fo_{79} and Fo_{74}.

The vertical variation in MgO through the GOPd (Fig. 6b) reflects the differential distribution of olivine and a similar variation in Mg# relates largely to the olivine/augite ratio. Likewise, the less systematic variation in Ca# (Fig. 5b) probably indicates changes in the relative amounts of plagioclase and augite rather than any fundamental internal differentiation within the unit. However, profiles for the $Mg\#_{Max}$ of olivine and augite through the unit are C-shaped (Henderson *et al.*, 2000, fig. 2), suggesting that the liquid from which these phases crystallized was less evolved in the central part of the unit than at the edges. Furthermore, the liquid at the lower margin of the GOPd appears to have been more evolved than that at the top.

The GOPds have similar hump-shaped REE profiles to the picrites and concentrations spanning the upper part of the range exhibited by the latter (Fig. 13a and e). Not surprisingly, the lowest concentrations of REE and incompatible elements occur in GOPds from the olivine-rich central part of the unit such as SC1040. All analysed samples, such as those shown in Fig. 14a, exhibit relative depletions in Nb. The lowest analysed sample from the

unit, SC1060T, is unusual in having a marked positive Eu anomaly (Fig. 13a), large peaks for Hf and Zr and an exceptionally large Nb depletion (Fig. 14a). This sample has been shown (Foland *et al.*, 2000) to be one of the most contaminated with material derived from the country rocks. The heterogeneous nature of the GOPds, and the fact that some of them contain ~10% normative *hy*, reflect the variable extent of this contamination.

The mineral, whole-rock and Sr–Nd isotope chemistry of the GOPds necessitate a complex emplacement and differentiation model. The unit was intruded as a magmatic suspension of olivine crystals at a time when the upper part of the underlying crinanite with which it came into contact was a relatively rigid crystal mush, but still contained significant quantities of liquid. The experiments of Philpotts & Carroll (1996) suggest the amount of liquid could have been up to 65%. By contrast, the overlying picrite was probably completely solid. The previous junction between the top of the crinanite and the bottom of the Upper Picrite was obliterated by the intrusion of the GOPd.

PARENTAL MAGMAS FOR THE INTRUSIVE UNITS

It has been shown (Gibb & Henderson, 1996; Foland *et al.*, 2000; Henderson *et al.*, 2000) that all of the units in the Shiant Isles sill were formed by intrusion of magmas containing substantial and variable amounts of suspended olivine crystals. A small amount of plagioclase was also introduced in this way but most of this mineral, and all of the augite, crystallized *in situ* after emplacement. We have used olivine modal proportions and compositions and whole-rock analyses to calculate the compositions of the liquids in which the olivine was suspended (= parental liquids) for different units in the sill. We also used the Cr contents of the rocks to deduce that approximately 1–2 wt % of the suspended material was spinel. The calculated liquids are subject to error but provide a useful first-order estimate of the intruded liquid compositions. Although a parent liquid is calculated for the olivine teschenites, the extensive alteration of this rock type calls into question its reliability, especially for alkalis and other mobile elements. We have not attempted to model a parental liquid for the GOPd because of the heterogeneity of the unit.

The data for four large-feldspar picrites from the central part of the Lower Picrite provide a model parent liquid (PicrPL, Table 2). These samples were chosen for their reliable modal data and because they come from the part of the Picrite with the most primitive liquid. Only olivine ($Fo_{82·7}$) and spinel components were subtracted to give PicrPL. The Mg# for this composition is 55·2. Similar calculations for five 'picrodolerites' (with ~50% modal olivine) from the bottom part of the Picrodolerite–crinanite give PdolPL1 with Mg# = 55·7 (Table 2). The compositions of PicrPL and PdolPL1 are very similar. Two olivine teschenites from the top of the sill give a parent liquid (OTPL, Table 2) with Mg# = 51·4. Another liquid composition, PdolPL2, was calculated by averaging three of the highest picrodolerites in the unit and subtracting a slightly more evolved olivine component (35% of $Fo_{79·2}$), together with 1% of spinel and 15% of plagioclase (An_{83}). This liquid has Mg# = 56·0, which is effectively the same as for PdolPL1, but PdolPL2 is slightly poorer in CaO and richer in SiO_2 and alkalis than both PdolPL1 and PicrPL. While these differences mainly reflect the onset of calcic plagioclase fractionation at this stage, the Sr and Nd isotope systematics (Foland *et al.*, 2000) indicate that crustal contamination may have contributed to them.

The liquid in equilibrium with $Fo_{82·7}$ should have Mg# = 58·9 [$(Fe:Mg)^{ol}/(Fe:Mg)^{Liq} = 0·30$ (Roeder & Emslie, 1970)]. The picrite and both picrodolerite parental liquids are within error of being in equilibrium with their suspended olivines but the modelled olivine teschenite liquid is clearly too evolved to have crystallized its olivine. Note that each of the parental liquids plots among the crinanites in variation diagrams such as Fig. 15. The positions of the parental liquids relative to the field boundaries (cotectics) in the olivine–plagioclase–augite system (Fig. 2a) are particularly significant. OTPL (Fig. 2a, circle 2) plots close to the olivine–plagioclase cotectic consistent with plagioclase being the second silicate phase to crystallize and with the phenocryst assemblage observed in the chilled margins (Fig. 7). PicrPL (Fig. 2a, circle 1), PdolPL1 (circle 3) and PdolPL2 (circle 4) all plot close to the 5 kbar ternary eutectic of Morse *et al.* (2004), indicating that the liquid phases of the phenocryst-laden magmas intruded to form the Picrite and Picrodolerite–crinanite units were very close to being saturated with augite in addition to olivine and plagioclase by the time they were emplaced into the sill. The establishment of this condition must have occurred in the lower level magma chamber(s) that fed the sill or in the feeder system(s), and probably in both.

The incompatible trace element contents of these parental liquids are calculated simply by scaling mean bulk-rock compositions for the amounts of crystalline phases subtracted. Representative trace element data are given in Table 2 and plotted on REE and incompatible trace element diagrams in Fig. 17. The patterns are more meaningful than the absolute concentrations and have therefore been normalized to the Yb value. PicrPL shows the characterisitic hump-shaped REE pattern in Fig. 17a (La/Gd = 0·71, Gd/Yb = 1·42) with no Eu anomaly. Figure 17b shows a smoothly sinuous shape except for a pronounced negative P anomaly and a small Ti anomaly; note the absence of anomalies for Th and Nb. PdolPL1 also has a hump-shaped REE pattern (La/Gd = 0·90,

Table 2: Compositions of modelled parental liquids

Oxide (wt.)	PicrPL	OTPL	PdolPL1	PdolPL2	Evolved crinanite†	Pegmatite SC1115
SiO_2	46·17	46·39	46·60	48·60	46·80	47·40
TiO_2	2·09	1·65	1·60	1·72	2·15	3·15
Al_2O_3	18·06	17·16	19·40	19·00	16·40	12·50
FeO*	11·27	12·79	10·10	8·99	12·90	16·40
MnO	0·19	0·19	0·17	0·13	0·21	0·27
MgO	6·77	6·56	6·19	5·62	4·13	2·66
CaO	13·45	11·88	13·60	12·52	10·70	8·89
Na_2O	2·53	2·71	2·74	3·00	3·36	3·95
K_2O	0·15	0·18	0·23	0·35	0·49	0·91
P_2O_5 (ppm)	0·14	0·16	0·14	0·14	0·21	0·95
Cr	519	307	460	322	50	4
Ni	468	94	301	583	47	20
Ba	72	47	90	140	149	284
Rb	4·3	3·4	8·5	8·3	9·3	23·0
Sr	298	305	286	449	272	219
Y	27	21	24	33	35	92
Zr	124	86	118	132	142	318
Nb	3·30	2·35	2·88	4·40	5·70	12·0
La	5·27	3·16	4·98	4·89	9·42	23·1
Gd	6·13	3·42	4·59	3·75	6·75	17·0
Yb	3·53	1·73	2·65	1·94	3·50	7·93
Hf	3·67	2·23	3·00	3·98	4·65	10·3
Th	0·45	0·21	0·62	0·74	0·96	1·64
U	0·11	0·07	0·20	0·20	0·18	0·45
Olivine Fo‡	80·8	78·2	81·1	81·4	69·1	53·6
Mg#	55·2	51·4	55·7	56·0	39·7	25·0
Ca#	73·9	69·9	72·2	68·2	61·6	51·9

*Total Fe as FeO. †Evolved crinanite = Average of S81/35, SC1397 and SC1464. ‡'Equilibrium' composition calculated from parent liquid Mg# using $(Fe:Mg)^{Ol}/(Fe:Mg)^{Liq} = 0{\cdot}30$ (Roeder & Emslie, 1970).

Gd/Yb = 1·41) but has a clear positive Eu anomaly (Fig. 17a) and negative anomalies for Nb, P and perhaps for Th and Ti (Fig. 17b). PdolPL2 has lost the downturn for the LREE (La/Gd = 1·08), but has a similar shape for HREE to that of PdolPL1 (Gd/Yb = 1·58) and a clear positive Eu anomaly with pronounced negative anomalies for Th, Nb, P and Ti.

The incompatible trace element differences between these three model liquids reflect processes occurring very early in the formation of the sill. Foland *et al.* (2000) showed that the Picrite had relatively uncontaminated Sr and Nd isotope ratios whereas the Picrodolerite–crinanite was contaminated, possibly with ~5% amphibolitic lower crust. They also deduced that the Sr–Nd isotope compositions indicated the magma at the top of the Lower Picrite had exchanged interstitial liquid with the lowermost overlying picrodolerites.

The relatively simple incompatible element pattern for PicrPL characterizes the original uncontaminated parent magma (i.e. no anomalies except for P). The pronounced negative anomalies for Th and Nb, and the positive Eu anomaly for PdolPL2, are assumed to be characteristic of the contaminated parent magma of the Picrodolerite–crinanite unit. Gibson (1990) discussed possible crustal contaminants in the differentiated mafic sills of northern Skye. She showed that both upper-crustal amphibolites and lower-crustal granulites from the local Lewisian have pronounced negative anomalies for Th and Nb, with some having positive Eu anomalies and all are LREE-enriched (Weaver & Tarney, 1980, 1981). Thus, many of the incompatible-element features of the Shiant Isles Picrodolerite–crinanite parent magma (PdolPL2) could have been produced by contamination of PicrPL by ~10% granulitic or amphibolitic country rock.

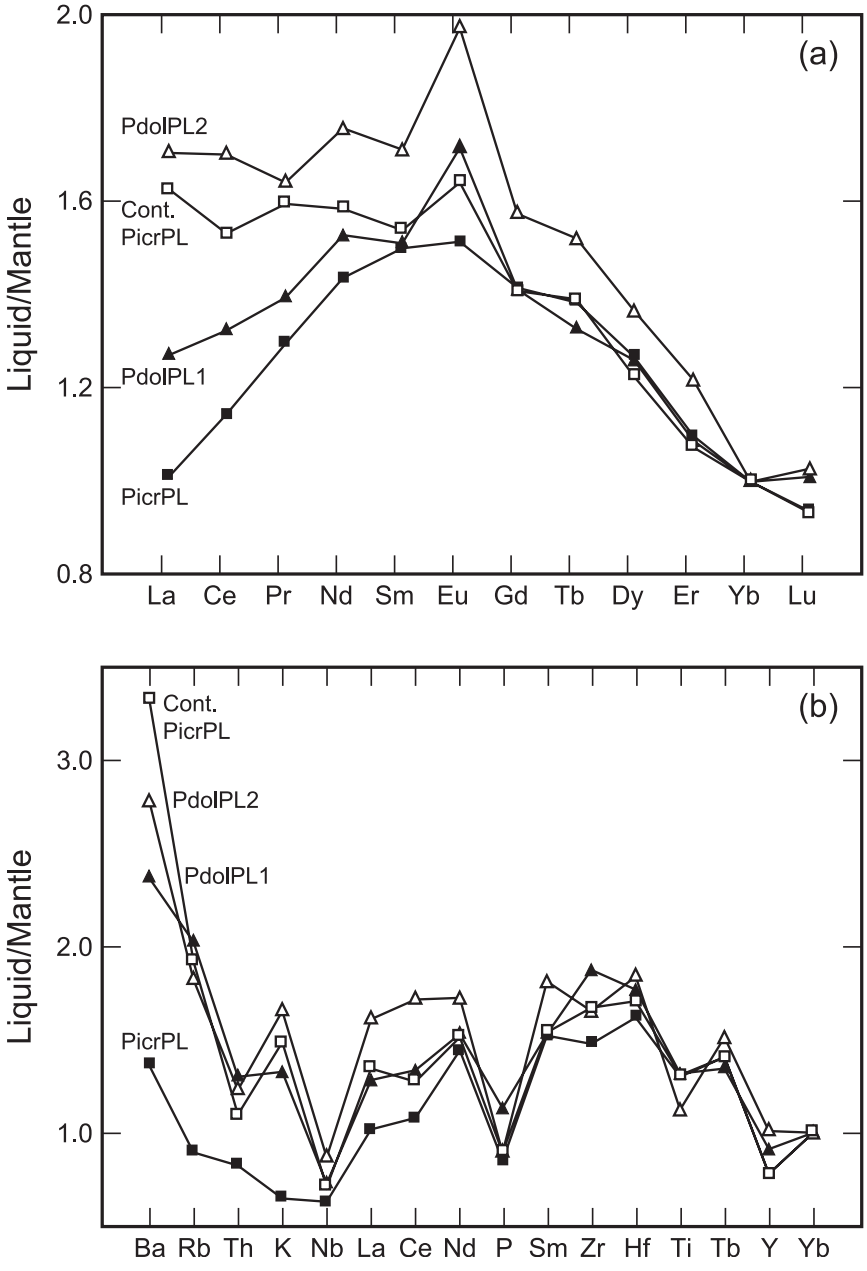

Fig. 17. (a) REE and (b) incompatible trace element diagrams for calculated parental liquid compositions (Table 2) normalized to the 'pyrolite' mantle of McDonough & Sun (1995). Element values are adjusted to Yb = 1 (see text). In (a) Cont.PicrPL is PicrPL contaminated with 10% intermediate amphibolite and 10% granulite; in (b) Cont.PicrPL is PicrPL with 5% each of the same contaminants (see text).

In Fig. 17b, the incompatible element pattern Cont.-PicrPL is for a contaminated picrite, with the contaminant consisting of 5% intermediate amphibolite and 5% granulite. Figure 17a shows the related REE trend but to produce this LREE pattern, it is necessary to use as the contaminant a mixture of 10% intermediate amphibolite and 10% granulite. Such a mixed crustal contaminant has Nd and Sr isotope systematics that would allow about 15% crustal contamination rather than the 5% acid amphibolite suggested by Foland *et al.* (2000). PdolPL1 has LREE contents and Th, Nb and Eu anomalies intermediate between those of PicrPL and PdolPL2. These features of PdolPL1 (which was derived from the lowermost picrodolerites) are consistent with the mixing of uncontaminated interstitial liquids from the Lower Picrite with contaminated liquid (PdolPL2) from the Picrodolerite–crinanite unit by exchange across the Lower Discontinuity (Foland *et al.*, 2000).

Table 3: Least-squares models for fractionation of parental liquid PdolPL1/2

	Model 1—PdolPL1/2 to evolved crinanite. Composition (wt %)		Model 2—Evolved crinanite to pegmatite. Composition (wt %)	
Parental liquid	PdolPL1/2		Evolved crinanite	
Olivine	Fo_{63}	7·8	Fo_{59}	6·7
Clinopyroxene	Mg# = 63	16·6	Mg# = 57	12·5
Plagioclase	An_{76}	41·7	An_{59}	39·4
Ti-Magnetite:Ilmenite	1:1	1·2	1:0	0·8
Apatite		−0·04		0·5
Residual liquid	Crinanite	32·7	Pegmatite	40·1
ΣR^2		0·23		0·16

Although the trace element patterns show significant variations between the different parental liquids, it is clear that the major element compositions of the liquid fractions of the Picrite and Picrodolerite–crinanite units are very similar (cf. Mg# and Ca#, Table 2). Therefore, the major element composition of the parental liquid that subsequently fractionated to produce the Picrodolerite–crinanite unit can be approximated by an average of PdolPL1 and PdolPL2 (= PdolPL1/2). We have used a least-squares mixing program (Bryan *et al.*, 1969) to model the fractionation of this composition through the most evolved crinanites (S81/35, SC1397 and SC1464) to the most evolved pegmatite (SC1115) (Table 3). The mineral extract compositions used (Table 4) were those from appropriate less evolved rocks than those being modelled. The sums of residuals are small, with most of the mismatch for the fractionation from PdolPL1/2 to the Evolved crinanite composition being for Na_2O, TiO_2 and P_2O_5. Because of the deuteric–hydrothermal analcimization (Foland *et al.*, 2000), it is assumed that the system is effectively open to Na for this model. By contrast, the model for the fractionation from the Evolved crinanite to pegmatite SC1115 fits perfectly for Na_2O and only TiO_2 and P_2O_5 show misfits. It is clear from both models that plagioclase is the dominant fractionating phase, followed by clinopyroxene. However, olivine (Fo_{77}–Fo_{45} (Gibb & Henderson, 1996)) is still an important crystallizing component, even at the pegmatite formation stage (Table 3), and this is confirmed by the presence of large (5–10 mm) crystals of olivine, often extensively altered, in the pegmatitic horizons (Fig. 3).

The relatively An-rich nature of fractionating plagioclase and the high Mg#s of olivine and clinopyroxene highlight the fact that whereas evolved rocks like the crinanites contain strongly zoned phases (Johnston, 1953; Gibb, 1973; Gibb & Henderson, 1996), the bulk-rock compositions do not show such extremes. Thus, although residual liquids became highly evolved *in situ*, they generally did not migrate. Hence, the Shiant Isles sill does not show wholesale concentration of evolved liquids in a 'sandwich horizon', and this is reflected in the limited development of pegmatitic facies. This is consistent with the lack of major Eu anomalies because residual liquids and fractionating (zoned) crystals were not separated from each other so that even the most evolved crinanites do not show significant Eu anomalies. Of all the samples studied, only pegmatite SC1115 shows a negative Eu anomaly; this is the only sample having geochemical features of an *extracted* residual liquid.

ORIGINS OF THE SHIANT ISLES MAGMAS

The igneous rocks most closely associated, temporally and spatially, with the sills of the Little Minch Sill Complex (LMSC) are the lavas of northern Skye, particularly the alkaline-transitional basalts of the Skye Main Lava Series (SMLS) (Thompson *et al.*, 1972). Indeed, Thompson *et al.* took the members of the LMSC intruded into the Jurassic sediments underlying the lava pile in Skye to be part of the SMLS "magmatic system". Gibson (1990) compared the Trotternish (N Skye) sills of the LMSC with the alkaline basalts of the SMLS and highlighted their geochemical similarity, especially in terms of their incompatible element and REE patterns. Although the sills are more olivine-rich and more contaminated with crustal material, she concluded that the parental magma of the sills was probably alkali olivine basalt very similar to an uncontaminated SMLS basalt. However, she contrasted the crustal contamination of the sills by amphibolite-facies gneiss with the apparently deeper-level contamination of the SMLS by granulite-facies material (Thirlwall & Jones, 1983).

Foland *et al.* (2000) recognized from the Nd and Sr isotope signatures that two different magmas were involved in the formation of the Shiant Isles sill: an isotopically more primitive "picritic" one that was parental to the Olivine Teschenite, Picrite and GOPd units and a more evolved "crinanitic" magma which gave rise to the Picrodolerite–crinanite unit. They suggested that the balance of evidence favoured a mantle origin for the former, with the latter being derived from it through contamination with amphibolite-facies gneiss, but to a lesser extent (~5%) than the 15–20% suggested by Gibson (1990) for the Trotternish sills.

The patterns exhibited by the incompatible trace elements in almost all Shiant Isles sill rocks (Fig. 14) can be interpreted as enrichments in Ba, Rb and K, as depletions in Th and Nb or as both. However, rocks from the central part of the Lower Picrite mostly lack Th and

Table 4: Mineral compositions used in least-squares modelling

	Model 1: PdolPL1/2 to Evolved crinanite					Model 2: Evolved crinanite to Pegmatite		
	Olivine S82/69	Clinopyroxene S82/69	Plagioclase S82/69	Ti-magnetite S82/69	Ilmenite SC533	Olivine S82/69	Clinopyroxene S82/69	Plagioclase S82/69
SiO_2	36·8	51·5	49·0	0·6	n.d.	36·6	51·1	53·4
Al_2O_3	n.d.	1·7	32·3	1·1	n.d.	n.d.	2·4	29·2
FeO	32·3	12·5	0·6	65·6	40·4	35·2	14·3	0·6
MnO	0·5	0·2	n.d.	n.d.	n.d.	n.d	n.d.	n.d.
MgO	30·8	12·0	n.d.	0·6	6·1	28·9	10·5	n.d.
CaO	0·5	20·8	15·3	n.d.	n.d.	0·4	20·2	12·3
Na_2O	n.d.	0·8	2·7	n.d.	n.d.	n.d.	0·8	4·6
K_2O	n.d.	n.d.	n.d.	n.d.	n.d.	n.d.	n.d.	0·1
TiO_2	n.d.	1·2	n.d.	30·2	52·0	n.d.	1·2	n.d.
Mole%	Fo_{63}	Mg# 63	An_{76}			Fo_{59}	Mg# 57	An_{59}

Nb depletion. There is also a small negative P anomaly. Similar incompatible element patterns were found for the Skye members of the LMSC (Gibson, 1990, fig. 5) and most basalts of the SMLS (Morrison *et al.*, 1980; Scarrow & Cox, 1995). Most of the sill rocks and many of the SMLS basalts show strong enrichments in Sr; however, in view of the hydrothermal origin for much of the Sr demonstrated by Foland *et al.* (2000), we do not attach any fundamental significance to this.

Most of the Shiant Isles rocks show enrichment in LREE relative to HREE. However, in the units formed from the "picritic" magma (Olivine Teschenite, Picrite and GOPd), the strongest enrichments are in Nd, Sm, Eu and Gd, i.e. there is a downturn in the LREE enrichment trend for La, Ce and Pr. Similar REE patterns have been recorded from the LMSC sills of N Skye (Gibson, 1990) and the SMLS basalts (Thompson *et al.*, 1980). However, the $(Ce/Yb)_N$ values for the Olivine Teschenite (1·37), Picrite (1·23), Picrodolerite–crinanite (1·70) and GOPd (1·45) are all lower than those typical of the SMLS basalts and the N Skye sills (3–4), indicating a lower degree of LREE enrichment in the Shiant Isles sill.

Kent & Fitton (2000) discriminated between four magma types (M1–M4) in the British Palaeogene Igneous Province using the immobile trace elements Ti, Y, Zr and Ce. The results of applying their approach to the Shiant Isles sill rocks are given in Table 5 but not every ratio for each rock type yields an unequivocal fit to the parameters given by Kent & Fitton; such cases are shown in italics. The greatest ambiguity centres on the Ce/Y ratio and this is almost certainly related to the lower degree of LREE enrichment in the sill rocks compared with, for example, the SMLS. Nevertheless, if the Shiant Isles rocks were formed from one of the four Palaeogene magma types, as would be assumed, it is clear from Table 5 that it has to be M1. Not surprisingly, M1 includes the SMLS and Mull Plateau Group lavas.

There is therefore a strong case for the premise that the "picritic" and "crinanitic" magmas involved in the formation of the Shiant Isles sill are related to each other, as postulated by Foland *et al.* (2000), and also that the "picritic" magma had ultimately a similar mantle origin to the other Hebridean M1 magmas, especially those of the SMLS and other LMSC sills. However, as the hump-shape of the picrite REE pattern is believed to represent an uncontaminated mantle-derived magma composition (above), it appears that the sill magmas were derived from a region of upper mantle that was more depleted in LREE than the source(s) of most of the Scottish Tertiary basaltic rocks. This is reflected in the Nd and Sr isotope ratios characteristic of the Shiant Isles picritic rocks (Foland *et al.*, 2000). Such extreme depletion in LREE relative to MREE seems to be quite unusual, but note that similar hump-shaped REE trends ($La/Gd \sim 0{\cdot}5$, $Gd/Yb \sim 1{\cdot}7$) have also been reported for komatiites from Finland (Hanski *et al.*, 2001).

Early studies of the SMLS chemistry (Thompson *et al.*, 1972, 1980; Morrison *et al.*, 1980) led to the conclusion that the more magnesian basalts were primary and formed by small fraction melting, at depths of between 60 and 80 km, of mantle material of variable composition from which less than 1% of material had previously been extracted as alkalic magmas. They attributed the SMLS to the earliest stages of melting associated with the thermal perturbation that initiated the opening of the North Atlantic Ocean. Later work (Scarrow & Cox, 1995; Scarrow *et al.*, 2000) suggested the SMLS basalts evolved

Table 5: Immobile trace element ratios and magma types

Rock type	Y/Zr			Ti/Zr			Ce/Y		
	Range	Mean	M-type	Range	Mean	M-type	Range	Mean	M-type
GOPd	0·09–0·26	0·22	M1	28–108	82	M1	0·47–0·66	0·54	*M1/M2*
Pegmatite	0·25–0·29	0·27	*M1/M2*	59–181	126	*?*	0·44–0·68	0·58	*M1/M2*
Crinanite	0·23–0·32	0·25	*M1/M2*	85–125	96	*M1/M2*	0·38–0·81	0·60	*M1/M2*
Picrodolerite	0·17–0·26	0·23	M1	64–99	85	M1	0·33–0·75	0·60	*M1/M2*
LF picrite	0·19–0·24	0·22	M1	77–102	88	*M1/M2*	0·40–0·60	0·50	*M1/M2*
MF picrite	0·21–0·24	0·22	M1	63–102	80	M1	0·39–0·73	0·49	*M1/M2*
SF picrite	0·17–0·29	0·22	M1	65–107	88	*M1/M2*	0·46–0·59	0·54	*M1/M2*
Ol. teschenite	0·22–0·25	0·24	M1	99–128	111	M3	0·43–0·47	0·45	*M1/M2*

by olivine fractionation from a range of picritic parental magmas (MgO = 13–15%) that were generated by decompressive melting of abnormally hot ($T_P \sim$ 1440°C) mantle of variable composition associated with the Icelandic plume. The melting was initiated in the garnet stability field, with segregation occurring between 60 and 112 km at 1390–1510°C. Eruption temperatures were ~1200°C and close to the 'plagioclase in' temperature, i.e. similar to what we have deduced for the Shiant Isles sill magmas.

Kent & Fitton (2000) presented evidence that magmas intruded and erupted in the Hebridean area between 61 and 58 Ma were derived from two sources, namely "Icelandic" plume mantle and N-MORB-type mantle. They used a parameter ΔNb, related to the Nb–Zr–Y systematics of Icelandic basalts, to determine the relative contributions of the two sources, with ΔNb > 0 implying "Icelandic" mantle and ΔNb < 0 indicating N-MORB-like depleted mantle source. According to Kent & Fitton, this largely overcomes the problems of source identification caused by crustal contamination, as crustal material can only lower ΔNb and so never make magma from an N-MORB source appear "Icelandic". Almost all of the 60–61 Ma M1-type lavas from the British Isles (including the SMLS) have ΔNb < 0, indicating a N-MORB-type depleted mantle source. All of the Shiant Isles sill rocks have negative ΔNb values with means for the intrusive units of −0·33 (Olivine Teschenite), −0·34 (Picrite), −0·24 (Picrodolerite–crinanite) and −0·32 (GOPd). All are consistent with the magmas being North Atlantic Igneous Province M1 type, with a predominantly LREE-depleted upper mantle N-MORB-type source. Kent & Fitton (2000) suggested that such magmas originated by up to 10% melting of garnet lherzolite previously depleted in Ti and that this "heterogeneous N-MORB like mantle formed the outer envelope of the ancestral Icelandic plume", which, at 61 Ma, lay under intact, unrifted lithosphere beneath the British Isles.

THE SINGLE PULSE MODEL

Latypov (2003*a*) has drawn attention to the fact that many mafic layered intrusions and sills exhibit marginal reversals that are mirror images of the normal fractionation that occurs in the layered series and upper border series of the layered intrusion or in the central part of the sill. These reversals result in the marginal rocks being some of the most evolved in the intrusion and in inward trends towards more primitive compositions. They tend to be highlighted by variations in the amount of modal olivine and whole-rock MgO, Cr and Ni contents. Latypov contended that "conventional mechanisms of magma differentiation" (including multiple intrusion) cannot provide "an adequate explanation for the characteristic features of the marginal reversals". He further suggested that their apparently widespread occurrence in a wide variety of shapes and sizes of intrusion supports an origin through the operation of a universal mechanism independent of gravity.

Latypov (2003*b*) cited the Shiant Isles sill as the type example of a sill with a "double humped" S-shaped profile. He divided such sills into four parts: a basal zone or reversal; a layered series; an upper border series; and a top zone or reversal (Fig. 18), and proposed that these form as follows. Chilled margins form initially on emplacement of the magma but are melted back by the high heat flux once vigorous internal convection becomes operational (Huppert & Sparks, 1989; Latypov, 2003*b*) and steep marginal temperature gradients are established. This is followed by a period in which Soret diffusion and component transfer produce more evolved liquids in the marginal boundary layers. As the sill solidifies inwards, these processes become less effective and the liquids gradually become less evolved, resulting in the basal and top reversals. By the time crystallization reaches the upper and lower "crossover maxima" (Fig. 18), the temperature gradients are too small for Soret diffusion and normal fractional crystallization

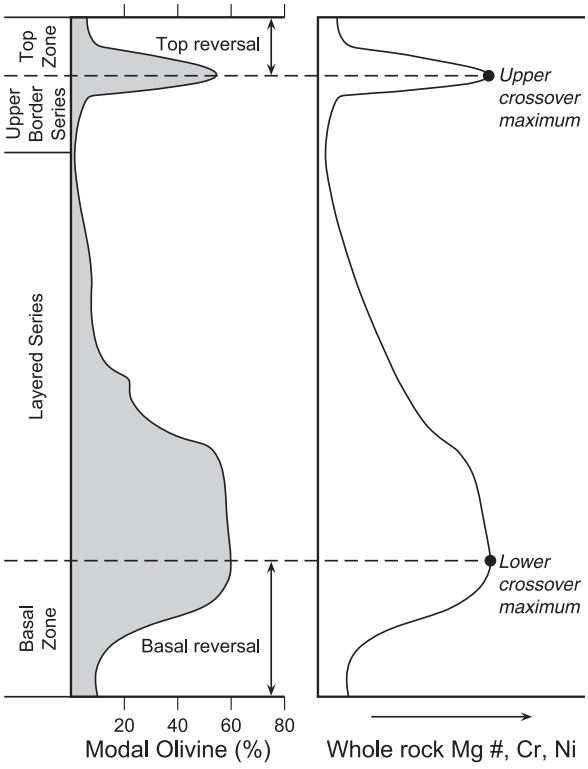

Fig. 18. The Latypov (2003) model of an idealized basic–ultrabasic sill with a "double humped" compositional profile (after Latypov, 2003*b*, fig. 9).

takes over to form the 'layered series' and 'upper border series' with the last, most evolved, liquids crystallizing at the junction between the two (for detailed explanation, see Latypov, 2003*b*, fig. 9). The crystallization of the entire sill is a single continuous event, with no interruptions or missing parts once the melt-back of the original chilled margins ceases.

It is not our intention here to question the petrogenetic viability of Soret diffusion or the mechanism proposed by Latypov but, by examining its applicability to the Shiant Isles Main Sill, to raise doubts about its wider relevance for large mafic sills. Solely for the purposes of this section, we shall accept two premises. First, that the mechanisms of sustained vigorous internal convection and Soret diffusion operating as proposed by Latypov might be feasible and, second (notwithstanding the evidence to the contrary), that the Shiant Isles sill was emplaced as a single pulse of phenocryst-free (or poor) magma.

Latypov (2003*a*) listed six "distinctive features of marginal compositional reversals … that impose strict constraints on any model for their formation". These are: (1) lack of mass balance between the outer parts of the marginal reversals and the bulk composition of the intrusion; (2) reversed order of phase crystallization; (3) reversed mineral composition trends compared with those in the main body of the intrusion; (4) the cotectic composition of the marginal reversal rocks; (5) their capacity to form from phenocryst-free, -poor or -rich magmas and (6) the ability to form independently of gravity on the floor, walls and roof of the magma chamber. It was the perceived inability of more conventional models to account for these features that led him to propose his internal convection and Soret diffusion-based model. We shall examine each of these in the context of the Shiant Isles sill and consider some other aspects relevant to the interpretation of the sill as a single-pulse intrusion formed as proposed by Latypov (2003*b*).

Mass balance

One of Latypov's (2003*a*) main justifications for seeking a new mechanism was that the chilled margins of most sills are not representative of the bulk composition of the intrusion. In the first place, the logic that it should be may be flawed. Why should the leading edge of a thin wedge of magma intruding along a bedding plane have exactly the same composition as the main bulk of the magma that follows it? As the sill and feeder widen with time and the passage of magma, the flow rate, temperature, content and distribution of any phenocrysts and, consequently, the composition of the magma are more likely to change than not. Expecting the chilled margins to have the same composition as the whole intrusion is akin to expecting the first drops of magma extruded from a volcano to be the same as the average composition of the lava throughout the eruption. Compositional variations during eruptions and zoned lava flows are not unusual.

There is no disputing that the compositions of the upper and lower chilled margins of the Shiant Isles sill do not correspond to the bulk composition of the sill as a whole. Because the actual margins of the sill are clearly chilled, represent the first magma emplaced into the sill and could not have formed after marginal melt-back (above), their very existence is incompatible with formation of the sill from a single injection of magma as proposed by Latypov (2003*b*). Consequently, an alternative explanation must be found for the lack of mass balance with the sill as a whole, the obvious candidate being multiple intrusion combined with other processes, as described in previous sections.

Phase sequence

In support of his model, Latypov (2003*a*) pointed out that chilled margins tend to be close to the lowest melting composition on the parental liquid line of descent. The lowest melting composition for a single-pulse Shiant Isles sill would be around the 125–135 m level (Fig. 3), where it is clear from the textural relations that olivine,

plagioclase, augite and Ti-magnetite crystallized together. By contrast, the chilled margins were, at the time of emplacement, on (and probably only just on) the Ol–Pl–Liquid cotectic (Fig. 2a). We have seen no evidence of any inverse order of crystallization in the margins of the sill.

Mineral compositions

Latypov highlighted the tendency for mineral compositions to become more primitive away from the margins throughout the basal and top reversals. There are certainly changes of this type away from the upper and lower margins of the Shiant isles sill for some parameters, e.g. $Mg\#_{Max}$ of augite (Gibb & Henderson, 1996; Henderson *et al.*, 2000), but not for others, e.g. $Mg\#_{Max}$ of olivine. However, treating the sill as a single intrusion, none of these "cryptic reversals" persists from the margin to the "crossover point" (Fig. 18) as required by the model.

Cotectic composition

According to Latypov, the outermost parts of the marginal reversals should have a modal mineralogy corresponding to the "proportions expected from liquids crystallizing along an Ol–Pl–Cpx–Liquid cotectic". In the system diopside–forsterite–anorthite at 1 atm (Fig. 2a; Osborn & Tait, 1952), the minimum liquidus composition is $Fo_{7.5}An_{43.5}Di_{49}$ compared with the values of $Ol_{10–17}Pl_{59–68}Cpx_{31–25}$ used by Latypov (2003*b*; e.g. fig. 12). A modal analysis for a Shiant sample ~1 m from the top of the sill (SC1008) has mineral proportions $Ol_{24}Pl_{50}Cpx_{26}$ compared with average CIPW values of $Ol_{24}Pl_{59}Cpx_{17}$ for three samples from the top teschenite unit. None of the analysed marginal olivine teschenites lies on or close to either the 1 atm or 5 kbar cotectics (Fig. 2a). These teschenites are from well within what Latypov (2003*b*) regarded as the outer parts of the marginal reversals in the Shiant Isles sill; however, it is clear that their compositions are far from that of a three-phase cotectic (Fig. 2a), and indeed fall in the Ol–Liquid field, as indicated by the rock texture (Fig. 7).

Phenocrysts

The model for the origin of a "double humped" sill from a single pulse of magma requires that all, or almost all, of the olivine crystallizes *in situ*, mostly along Ol–Pl and Ol–Pl–Cpx cotectics. In support of this model, Latypov (2003*b*) presented a number of arguments from which he concluded that the "size, morphology and composition of phenocrysts in the chilled margins of sills present no compelling evidence for their intratelluric origin". We are not convinced by these arguments and have already made the case that olivine phenocrysts were present in all of the Shiant Isles sill magmas at the time of their emplacement—a case that is especially strong for the chilled margins. Further, it is evident from their $Mg\#_{Max}$ values that the olivine and augite throughout much of the sill did not form through equilibrium crystallization along a cotectic (Henderson *et al.*, 2000), supporting our previously stated view that the more primitive olivine phenocrysts ($\sim Fo_{83}$) were introduced with the magma whereas the pyroxenes crystallized entirely *in situ*.

Gravity

Latypov also argued against the formation of sills with S-shaped profiles by any form of physical redistribution of introduced phenocrysts or early formed crystals such as gravity settling or flow differentiation. In particular, he stated "the occurrence of two maxima in olivine concentration in some sills" (including the Shiant Isles) "is difficult to reconcile with a gravity-controlled settling model involving a single magma pulse". We agree, but this is an argument against a single pulse, and not against gravity settling.

He further suggested that the change from higher olivine contents to around 15% in the 'layered series' part of the sill relates to the crystallization moving from the Ol–Liquid field onto the Ol–Pl–Liquid cotectic. Such a change would be fairly sudden and could not account for the gradual upward decrease in the olivine content through some 40 m of picrodolerite in the Shiant Isles sill (Fig. 3). Neither is the occurrence of the radiating clusters of plagioclase phenocrysts in these rocks (Gibb & Henderson, 1996) compatible with crystallization in the Ol–Liquid field. Indeed, gravity settling of early (largely introduced) olivines within the Picrodolerite–crinanite unit of our multiple intrusion is the only mechanism we can envisage for such a transition.

Margin melt-back

Lack of mass balance between the margins of a sill and its bulk composition was regarded by Latypov (2003*a*, 2003*b*) as evidence that the marginal facies formed "after olonged and extensive melt-back" of initial chilled margins. Such marginal melt-back is a consequence of the vigorous internal wholesale convection essential to the Latypov model, and should be more effective at the upper margin than the lower one (Huppert & Sparks, 1989). Quite apart from the fact that the margins of the Shiant Isles sill are chilled and show no evidence of melt-back, the upper and lower chilled margins are chemically and petrographically identical. This is incompatible with the convection and differential melt-back fundamental to the single pulse model.

"Crossover maxima"

Latypov's model for a "double humped" sill (Fig. 18) requires not only that there be two maxima in modal olivine, MgO, etc., but that they be of equal amplitude

because they represent equivalent horizons at the top and bottom of the sill at which Soret diffusion controlled fractionation gives way to normal fractional crystallization. The vigorous internal convection would guarantee this by ensuring the temperature and composition of the magma at two contemporaneous solidification fronts (at the crossover maxima) remained the same. The Shiant Isles sill cannot be made to fit this model.

In the first place, it is clear from Figs. 3 and 6 that there are at least four maxima in modal olivine, MgO and Ni in the sill. One, possibly two, occur(s) in the large-feldspar picrite of the Lower Picrite unit: one in the picrodolerite immediately above the Lower Discontinuity; one in the central part of the GOPd; and one in the medium-feldspar picrite above the Upper Discontinuity. Second, irrespective of which pair of maxima is chosen, the symmetry required by the Latypov model is conspicuously absent.

Further, according to the model, the minerals at the crossover maxima should have the most primitive compositions found anywhere throughout the sill. Although this is almost true of the modal maximum in the Lower Picrite unit, it is certainly not the case for any of the others. Also, as Latypov (2003*b*) pointed out, a feature of the upper olivine-rich unit in a "double humped" sill is that the compositions within it span the entire compositional range found throughout the whole intrusion. This is clearly not so for the Shiant Isles sill. There are no rocks from the upper half of the sill that exhibit compositions as primitive as the most olivine-rich picrites from the Lower Picrite (Figs. 5 and 6).

Compositional breaks

Latypov (2003*b*) questioned the interpretation of junctions between units marked by textural and grain-size changes as internal chills and, hence, as evidence of multiple injection in intrusions such as the Shiant Isles sill. He did, however, accept as "impressive evidence" for multiple injection the occurrence of reversals in normal fractionation trends. It is perhaps worth pointing out that with multiple intrusion, a reversal would occur only if the later magma was more primitive than the earlier one. In the case of the later magma being more evolved, there might be a compositional break in the fractionation trend but it would not be a reversal. Such breaks could conceivably arise from any gap in, disruption of, or partial removal of the products of, normal fractionation—but it is hard to envisage a realistic cause of such events in a sill other than a fresh injection of magma. Consequently, a compositional break in a fractionation trend, in either sense, can be taken as a reliable indication of multiple intrusion.

It is difficult to reconcile the compositional breaks in the Shiant Isles sill documented above, some of which are reversals and some not, with anything but multiple intrusion. Further, their coincidence with the petrographic breaks described previously (Gibb & Henderson, 1989, 1996; Henderson *et al.*, 2000) refutes the suggestion that textural and grain-size breaks are unreliable evidence of multiple intrusion. Equally, the compositional breaks are wholly inconsistent with any petrogenetic process or model involving continuous crystallization of a single body of magma.

DISCUSSION

Latypov further refined his model to demonstrate that different sill profiles would be formed, depending on the temperature difference across the marginal liquid boundary layers and the composition of the magma. Of these variants, the one that best fitted a "double humped" sill like the Shiant Isles involved a "super-cotectic" magma (Latypov, 2003*b*, fig. 12c). The model requires this magma to have been at the Ol–Pl–Cpx–Liquid eutectic during the formation of the sill margins. It is quite clear from the actual chilled olivine teschenite margins of the sill that this was not so (Fig. 2a).

It is obvious that the Shiant Isles sill cannot be fitted to the single pulse model. The more closely the sill is scrutinized in the context of the model, the more inconsistencies and contradictions emerge. By way of a final comment on the issue of single versus multiple intrusion, Sr and Nd isotope data (Foland *et al.*, 2000) demonstrate that two isotopically distinct magmas were involved in the formation of the sill—this is incontrovertible evidence. One of the principal objections to the formation of S-shaped sills, in general, by multiple injections of magma is that it is based on "accidental" events requiring too high a degree of coincidence in the light of how commonly they occur [see the discussion on the alkaline sills of northern Skye by Latypov (2003*b*, p. 1626)]. We beg to differ. While the Shiant Isles sill may be *slightly* unusual in that its formation involved *four* injections of magma, all that is necessary to generate most of the sill profiles featured by Latypov are two phases of intrusion. The precise profile produced depends mainly on the differences in composition and history of the magmas, their relative volumes and in what position in the first intrusion the second was emplaced.

We would anticipate that the normal process for filling a sill, or a unit within a multiple sill, would begin slowly as the thin leading edge of the magma forces apart the concordant fissure, and then speed up as injection progresses with the ever-widening gap between floor and roof allowing faster and faster flow until the magma pressure decreases. Under such conditions, the later, more centrally emplaced portions of the magma would be more likely to contain a higher concentration of any introduced phenocrysts and to transport them further

into the sill (cf. Fig. 4, Stages 2a and 2b). Whether or not, and to what extent, any such phenocrysts might subsequently be redistributed, e.g. by gravity, would depend on a variety of factors including temperature, density and viscosity of the magma and thickness of the unit.

We cannot avoid the comparison between the manner in which a large mafic sill is filled and volcanic eruptions. Basaltic eruptions are almost invariably protracted (lasting from days to years), episodic (i.e. pulsed) and frequently feature temporal changes in the crystallinity and composition of the magmas over the period of the eruption (e.g. Murata & Richter, 1966). We see no reason why this pattern should be the norm for mafic magmas reaching the Earth's surface but be regarded as an untenable coincidence when the magma is emplaced laterally below the surface to form a sill.

We conclude that, irrespective of whether or not Latypov's convection–diffusion model is applicable to other types of mafic–ultramafic intrusion, it did not operate in the case of the Shiant Isles sill, and we believe that all the available evidence supports our previous interpretation of this classic sill as a multiple intrusion. It is significant that, with few exceptions, whenever the chemistry of a large mafic sill has been investigated in sufficient detail, it has turned out to be the product of a complex (usually multiple) intrusive process, e.g. Shiant Isles, Lugar, Palisades. Consequently, far from being a type example of the controversial genetic mechanism for sills proposed by Latypov (2003*b*), we predict that the Shiant Isles sill will fulfil this role for a class of large (>∼50 m thick) mafic sills formed by multiple intrusion. This class will grow as the internal chemistries of further examples are investigated.

ACKNOWLEDGEMENTS

We are grateful to Mike Cooper for drafting the figures, Ray Kanaris-Sotiriou for XRF analyses, Paul Lythgoe and Nick Pearce for ICP-MS analyses, and Ken Foland for isotope dilution data and numerous discussions on sill chemistry. We thank Bruce Marsh, Tony Morse, Troels Neilsen and Marjorie Wilson for perceptive comments and improvements to the manuscript, Adam Nicolson for permission to undertake fieldwork, and Sally Gibson for information relating to the N Skye sills.

SUPPLEMENTARY DATA

Supplementary data for this paper are available at *Journal of Petrology* online.

REFERENCES

Berlin, R. & Henderson, C. M. B. (1969). The distribution of Sr and Ba between alkali feldspar, plagioclase and groundmass phases of porphyritic trachytes and phonolites. *Geochimica et Cosmochimica Acta* **33**, 247–255.

Brooks, C. K. (1977). The Fe_2O_3/FeO ratio of basalt analyses: an appeal for a standardized procedure. *Bulletin of the Geological Society of Denmark* **25**, 117–120.

Bryan, W. B., Finger, L. W. & Chayes, F. (1969). Estimating proportions in petrographic mixing equations by least squares approximation. *Science* **163**, 926–927.

Corrigan, G. M. (1982). Cooling rate studies of rocks from two basic dykes. *Mineralogical Magazine* **46**, 387–394.

Deer, W. A., Howie, R. A. & Zussman, J. (1978). *Rock-Forming Minerals: Vol. 2a, Single Chain Silicates*. Harlow: Longman.

Dickin, A. P., Henderson, C. M. B. & Gibb, F. G. F. (1984). Hydrothermal Sr contamination of the Dippin Sill, Isle of Arran, Western Scotland. *Mineralogical Magazine* **48**, 311–322.

Donaldson, C. H. (1976). An experimental investigation of olivine morphology. *Contributions to Mineralogy and Petrology* **57**, 187–213.

Drever, H. I. (1953). A note on the field relations of the Shiant Isles picrite. *Geological Magazine* **90**, 159–160.

Drever, H. I. & Johnston, R. (1957). Crystal growth of forsteritic olivine in magmas and melts. *Transactions of the Royal Society of Edinburgh* **63**, 289–315.

Drever, H. I. & Johnston, R. (1959). The lower margin of the Shiant Isles Sill. *Quarterly Journal of the Geological Society, London* **114**, 343–365.

Drever, H. I. & Johnston, R. (1965). New petrographical data on the Shiant Isles picrite. *Mineralogical Magazine* **34**, 194–203.

Foland, K. A., Gibb, F. G. F. & Henderson, C. M. B. (2000). Patterns of Nd and Sr isotopic ratios produced by magmatic and post-magmatic processes in the Shiant Isles Main Sill, Scotland. *Contributions to Mineralogy and Petrology* **139**, 655–671.

Gibb, F. G. F. (1973). The zoned clinopyroxenes of the Shiant Isles sill. *Journal of Petrology* **14**, 203–230.

Gibb, F. G. F. & Gibson, S. A. (1989). The Little Minch Sill Complex. *Scottish Journal of Geology* **25**, 367–370.

Gibb, F. G. F. & Henderson, C. M. B. (1978). The petrology of the Dippin Sill, Isle of Arran. *Scottish Journal of Geology* **14**, 1–27.

Gibb, F. G. F. & Henderson, C. M. B. (1984). The structure of the Shiant Isles sill complex. *Scottish Journal of Geology* **20**, 21–29.

Gibb, F. G. F. & Henderson, C. M. B. (1989). Discontinuities between picritic and crinanitic units in the Shiant Isles sill: evidence of multiple intrusion. *Geological Magazine* **126**, 127–137.

Gibb, F. G. F. & Henderson, C. M. B. (1992). Convection and crystal settling in sills. *Contributions to Mineralogy and Petrology* **109**, 538–545.

Gibb, F. G. F. & Henderson, C. M. B. (1996). The Shiant Isles Main Sill: structure and mineral fractionation trends. *Mineralogical Magazine* **60**, 67–97.

Gibson, S. A. (1990). The geochemistry of the Trotternish sills, Isle of Skye: crustal contamination in the British Tertiary Volcanic Province. *Journal of the Geological Society, London* **147**, 1071–1081.

Gibson, S. A. & Jones, A. P. (1991). Igneous stratigraphy and internal structure of the Little Minch Sill Complex, Trotternish Peninsula, northern Skye, Scotland. *Geological Magazine* **128**, 51–66.

Govindaraju, K. (1989). 1989 compilation of working values and sample description for 272 geostandards. *Geostandards Newsletter* **13**, 1–113.

Hanski, E., Huhma, H., Rastas, P. & Kamenetsky, V. S. (2001) The Palaeoproterozoic komatiite–picrite association of Finnish Lapland. *Journal of Petrology* **42**, 855–876.

Henderson, C. M. B., Gibb, F. G. F. & Foland, K. A. (2000). Mineral fractionation and pre- and post-emplacement processes in the uppermost part of the Shiant Isles Main Sill. *Mineralogical Magazine* **64**, 779–790.

Huppert, H. E. & Sparks, R. S. J. (1980). The fluid dynamics of a basaltic magma chamber replenished by influx of hot dense ultrabasic magma. *Contributions to Mineralogy and Petrology* **75**, 279–289.

Huppert, H. E. & Sparks, R. S. J. (1989). Chilled margins in igneous rocks. *Earth and Planetary Science Letters* **92**, 397–405.

Johnston, R. (1953). The olivines of the Garbh Eilean sill, Shiant Isles. *Geological Magazine* **90**, 161–171.

Kent, R. W. & Fitton, J. G. (2000). Mantle sources and melting dynamics in the British Palaeogene Igneous Province. *Journal of Petrology* **41**, 1023–1040.

Latypov, R. (2003*a*). The origin of marginal compositional reversals in basic–ultrabasic sills and layered intrusions by Soret fractionation. *Journal of Petrology* **44**, 1579–1618.

Latypov, R. (2003*b*). The origin of basic–ultrabasic sills with S-, D-, and I-shaped compositional profiles by *in situ* crystallization of a single input of phenocryst-poor parental magma. *Journal of Petrology* **44**, 1619–1656.

Le Maitre, R. W., Bateman, P., Dudek, A., Keller, J., Lameyre, J., Le Bas, M. J., *et al.* (1989). *A Classification of Igneous Rocks and Glossary of Terms: Recommendations of the International Union of Geological Sciences Subcommission on the Systematics of Igneous Rocks*. Oxford: Blackwell Scientific.

Marsh, B. D. (1989). On convective style and vigor in sheet-like magma chambers. *Journal of Petrology* **30**, 479–530.

Marsh, B. D. (1996). Solidification fronts and magmatic evolution. *Mineralogical Magazine* **60**, 5–40.

McDonough, W. F. & Sun, S.-S. (1995). The composition of the Earth. *Chemical Geology* **120**, 223–253.

Morrison, M. A., Thompson, R. N., Gibson, I. L. & Marriner, G. F. (1980). Lateral chemical heterogeneity in the Palaeocene upper mantle beneath the Scottish Hebrides. *Philosophical Transactions of the Royal Society of London, Series A* **297**, 229–244.

Morse, S. A., Brady, J. B. & Sporleder, B. A. (2004). Experimental petrology of the Kiglapait intrusion: cotectic trace for the lower zone at 5 kbar in graphite. *Journal of Petrology* **45**, 2225–2259.

Murata, K. J. & Richter, D. H. (1966). Chemistry of the lavas of the 1959–60 eruption of Kilauea volcano, Hawaii. *US Geological Survey, Professional Paper* 537-A.

Murray, R. J. (1954*a*). The clinopyroxenes of the Garbh Eilean sill, Shiant Isles. *Geological Magazine* **91**, 17–31.

Murray, R. J. (1954*b*). A detailed chemical and petrological investigation of the rocks of the Shiant Isles. Ph.D. thesis, University of St Andrews.

Nicolson, A. (2001). *Sea Room: An Island Life*. London: HarperCollins.

Osborn, E. F. & Tait, D. B. (1952). The system Diopside–Forsterite–Anorthite. *American Journal of Science, Bowen Volume*, 413–433.

Pearce, N. J. G., Perkins, W. T., Westgate, J. A., Gorton, M. P., Jackson, S. E., Neal, C. R. & Chenery, S. P. (1997). A compilation of new and published major and trace element data for NIST SRM 610 and NIST SRM 612 glass reference materials. *Geostandards Newsletter* **21**, 115–144.

Philpotts, A. R. & Carroll, M. (1996). Physical properties of partly melted tholeiitic basalt. *Geology* **24**, 1029–1032.

Philpotts, A. R., Brustman, C. M., Shi, J., Carlson, W. D. & Denison, C. (1999). Plagioclase-chain networks in slowly cooled basaltic magma. *American Mineralogist* **84**, 1819–1829.

Philpotts, J. A. & Schnetzler, C. C. (1970). Phenocryst–matrix partition coefficients for K, Rb, Sr and Ba with applications to anorthosite and basalt genesis. *Geochimica et Cosmochimica Acta* **34**, 307–322.

Roeder, P. L. & Emslie, R. F. (1970). Olivine–liquid equilibrium. *Contributions to Mineralogy and Petrology* **29**, 275–289.

Scarrow, J. H. & Cox, K. G. (1995). Basalts generated by decompressive adiabatic melting of a mantle plume: a case study from the Isle of Skye, NW Scotland. *Journal of Petrology* **36**, 3–22.

Scarrow, J. H., Curran, J. M. & Kerr, A. C. (2000). Major element records of variable plume involvement in the North Atlantic Province Tertiary flood basalts. *Journal of Petrology* **41**, 1155–1176.

Thirlwall, M. F. & Jones, N. W. (1983). Isotope geochemistry and contamination mechanics of Tertiary lavas from Skye, Northwest Scotland. In: Hawkesworth, C. J. & Norry, M. J. (eds) *Continental Basalts and Mantle Xenoliths*. Nantwich: Shiva, pp. 186–208.

Thompson, R. N., Esson, J. & Dunham, A. C. (1972). Major element chemical variation in the Eocene lavas of the Isle of Skye, Scotland. *Journal of Petrology* **13**, 219–253.

Thompson, R. N., Gibson, I. L., Marriner, G. F., Mattey, D. P. & Morrison, M. A. (1980). Trace-element evidence of multistage mantle fusion and polybaric fractional crystallization in the Palaeocene lavas of Skye, NW Scotland. *Journal of Petrology* **21**, 265–293.

van Zyl, C. (1982). Rapid preparation of robust pressed powder briquettes containing a styrene and wax mixture as a binder. *X-ray Spectrometry* **11**, 29–31.

Wager, L. R. & Brown, G. M. (1967). *Layered Igneous Rocks*. Edinburgh: Oliver & Boyd.

Walker, F. (1930). The geology of the Shiant Isles (Hebrides). *Quarterly Journal of the Geological Society, London* **86**, 355–398.

Weaver, B. L. & Tarney, J. (1980). Rare earth geochemistry of Lewisian granulite-facies gneisses, northeast Scotland: implications for the petrogenesis of the Archean lower continental crust. *Earth and Planetary Science Letters* **51**, 279–296.

Weaver, B. L. & Tarney, J. (1981). Lewisian gneiss geochemistry and Archean crustal development models. *Earth and Planetary Science Letters* **55**, 171–180.